Negative microfilm
received from university

63–312

BARROWS, John Frederick, 1928–
THEORETICAL AND EXPERIMENTAL ANALYSIS
OF FLUID FLOW SEPARATION.

University of Michigan, Ph.D., 1962
Engineering, mechanical

University Microfilms, Inc., Ann Arbor, Michigan

THEORETICAL AND EXPERIMENTAL ANALYSIS OF FLUID FLOW SEPARATION

John Frederick Barrows

A dissertation submitted in partial fulfillment
of the requirements for the degree of
Doctor of Philosophy in the
University of Michigan
1962

Doctoral Committee:

Associate Professor Arthur G. Hansen, Chairman
Associate Professor Vedat S. Arpaci
Doctor Craig Marks, General Motors Corp. Engineering Staff
Associate Professor Donald E. Rogers
Professor Chia-Shun Yih

PREFACE

The problem of flow separation has been recognized as an important one for many years. In contrast to its importance there has been little work done in this area of fluid mechanics. One of the major reasons is the difficulty of formulating the problem so that it will be amenable to analysis. The flow behavior, in general, is complicated especially in the regions which lie downstream of separation. When the author initially undertook this study, it was believed that little work had been done on this particular class of flow geometries. Further investigation revealed the work of M. J. Lighthill. Still further study convinced the author that an extension and evaluation of Lighthill's work would be beneficial, as many questions remained unanswered. It is believed that the following work will give insight into the problem and the limitations of the analysis. There are many valuable areas of work still remaining untouched in the general problem of corner flows, as the following analysis treats the flow outside the separated region.

The completion of this work marks the end of a formal period of study for the author. There are many people to whom the author owes a great deal. Although space does not permit that everyone can be mentioned, a few deserve special recognition. The author owes much to his parents for guidance and assistance throughout his entire period of formal education. The author would like to thank Professor A. G. Hansen, his advisor, for his encouragement and help in all stages of this work. Special thanks must go to the author's wife and children for their loving devotion, patience, and sacrifice.

TABLE OF CONTENTS

		Page
PREFACE		ii
LIST OF FIGURES		iv
NOMENCLATURE		vi
CHAPTERS		
I	INTRODUCTION	1
II	POTENTIAL FLOW SOLUTION FOR EXTERNAL FLOW	9
	A. Mathematical Solution	9
	B. Calculation of Lighthill's Solution	28
	C. Scheme of Calculation	31
	D. Configurations Used for Evaluation	32
III	VISCOUS SOLUTION	35
	A. Görtler's Series Solution	35
	B. Witting's Finite Difference Solution	38
	C. Application of Gortler's Series and Witting's Finite Difference Method	45
IV	EXPERIMENTAL INVESTIGATION	54
	A. Basic Test Equipment	54
	B. Test Channels	56
	C. Test Instrumentation	58
	1. Talcum Powder Generator	58
	2. Smoke Generator	60
	3. Static Pressure Instrumentation	62
	4. Pressure Recording	65
	5. Temperature Recording	69
	D. Experimental Program	69
	1. China Clay Technique	69
	2. Smoke Traces	72
	3. Talcum Powder and Oil Technique	78
	4. Static Pressure Measurements	82
	E. Comparison of Experimental Results	96
V	RESULTS AND CONCLUSIONS	99
	A. Results	99
	B. Conclusions	104
BIBLIOGRAPHY		105

LIST OF FIGURES

Figure		Page
1	Scale Drawing of the Channel Configurations, Showing Analytical Separation Points.....	34
2	$\bar{U}(\bar{x})$ vs. $\bar{x}$ for Configuration Number 1.....	47
3	$\frac{\partial \bar{u}}{\partial \bar{y}}\Big\|_{\bar{y}=0}$ vs. $\bar{x}$ for Configuration Number 1.....	51
4	Plot of $\frac{\partial \bar{u}}{\partial \bar{y}}\Big\|_{\bar{y}=0}$ vs. $\bar{x}$ for Analytical Velocity $\bar{U}(\bar{x})$ for Configuration Number 1.....	53
5a	View of Filter Assembly and Control Valve at Plenum Chamber Entrance.....	55
5b	View of Test Channel and Instrumentation.....	55
6	Typical Build Up of Test Section Showing Static Pressure Instrumentation.....	59
7	Schematic of Smoke Generator.....	61
8	View of Static Pressure Hole Locations.....	64
9a	View of Bottom of Test Section Showing Static Pressure Instrumentation.....	66
9b	View of Test Section Showing Static Pressure Instrumentation.....	66
10	Chattock-Fry Tilting Manometer.....	68
11a	China Clay Pattern with Configuration Number 1.....	71
11b	China Clay Pattern with Configuration Number 2.....	71
12a	Drying Pattern of China Clay After Five Minutes of Elapsed Drying Time.....	73
12b	Drying Pattern of China Clay After Ten Minutes of Elapsed Drying Time.....	73
12c	Drying Pattern of China Clay After Twenty Minutes of Elapsed Drying Time.....	74
12d	Drying Pattern of China Clay After Thirty-Five Minutes of Elapsed Drying Time.....	74

LIST OF FIGURES (CONT'D)

Figure		Page
13	Photographs of Smoke Traces Highlighting the Vortex Region.....	75-77
14a	Talcum Powder and Oil Technique for Configuration Number 1.....	79
14b	Talcum Powder and Oil Technique for Configuration Number 2.....	79
14c	Talcum Powder and Oil Technique for Configuration Number 3.....	80
15	Static Pressure Correction vs. Hole Number.....	84
16	Static Pressure Variation Along Horizontal Plate of Configuration Number 1.....	85
17	Static Pressure Variation Along Horizontal Plate of Configuration Number 2.....	86
18	Static Pressure Variation Along Horizontal Plate of Configuration Number 3.....	87
19	Plot of Dimensionless Velocity vs. Dimensionless Distance for Analytical and Experimental Results of Configuration Number 1.....	89
20	Plot of Dimensionless Velocity vs. Dimensionless Distance for Analytical and Experimental Results of Configuration Number 2.....	90
21	Plot of Dimensionless Velocity vs. Dimensionless Distance for Analytical and Experimental Results of Configuration Number 3.....	91
22	$\frac{\partial \bar{u}}{\partial \bar{y}}\Big\|_{\bar{y}=0}$ vs. $\bar{x}$ for Configuration Number 1.....	94
23	Plot of $\frac{\partial \bar{u}}{\partial \bar{y}}\Big\|_{\bar{y}=0}$ vs. $\bar{x}$ for Experimental Velocity $\bar{U}(\bar{x})$ for Configuration Number 1.....	95
24	Scale Drawing of the Channel Configurations, Showing Analytical and Two Experimental Separation Points.....	100
25	Plot of Free Streamline for Configuration Number 1 Using Static Pressure Test Data.....	103

NOMENCLATURE

Symbols used for potential solution

A, B, C, D, E, F	points in the flow field
a	vertical distance from corner to the reattachment point
b	distance along horizontal plate from separation point to corner
c	distance along horizontal plate from leading edge to separation point
h	vertical height of obstacle
i	$\sqrt{-1}$
$\overline{K}$	constant of integration
$\overline{L}$	constant of integration
K	complete elliptic integral $K = \int_0^{\pi/2} \frac{d\theta'}{\sqrt{1-k^2\sin^2\theta'}}$
K'	complete elliptic integral with modulus k'
k	modulus of elliptic integral $k = \sqrt{\frac{N}{M}}$
k'	complimentary modulus $k' = \sqrt{1-k^2}$
l	length of horizontal plate $a + b$
M	$\alpha - 1$
N	$\beta - 1$
P	constant
q	velocity magnitude
S	distance from B to C along the free streamline B-C
nS	distance from B to D along the line B-C-D
s	distance from point B to any point on the line B-C-D-E
t	transformation variable $w = \frac{UY}{\pi}\ell nt$
U	velocity of flow in upstream direction
u	velocity component in x direction

V	velocity along the free streamline B-C
v	velocity component in y direction
W	velocity along the free streamline D-E
w	complex potential $\phi + i\Psi$
X	$X = (\int_o^{nS} qds)/nS$
x	coordinate direction along plate
x'	variable $x' = (t-1)^{1/2}$
Y	channel depth
y	coordinate direction normal to plate
y'	variable
Z	distance between points E and F in x-y coordinate plane
z	complex variable $z = x + iy$
z'	variable $\ell n\ q/V$
α, β, γ	points in t plane corresponding to points B, C, D respectively in x-y plane
$\lambda, \mu, \eta, \epsilon$	exterior angles in Ω plans
θ	angle of flow measured with respect to the positive x axis
θ'	variable $\sin^{-1} x'/\sqrt{N}$
Γ	angle of the obstacle measured with respect to the positive x axis
ϕ	potential function
Ψ	stream function
Ω	transformation variable $\ell n\ dw/dz$

Symbols used by Görtler in his series solution

$F(\xi\eta)$ function $F(\xi, \eta) = \dfrac{\Psi(x,y)}{\left\{2\nu\int_o^x U(x)dx\right\}^{1/2}}$

$\bar{F}_k$	dimensionless function $F_k Re^k$
$\bar{g}(\bar{x})$	dimensionless function $\bar{U}(\bar{x})/\sqrt{2\bar{\xi}(\bar{x})}$
k	exponents $(k = 0, 1, 2, \ldots \infty)$
Re	Reynold's number $U_o h/\nu$
$U(x)$	velocity of outer flow
U_o	velocity at leading edge
$\bar{U}(\bar{x})$	dimensionless velocity $\bar{U}(\bar{x}) = \frac{u(x)}{U_o}$
u_k	coefficients of the polynomial $\sum_{k=o}^{\infty} u_k x^k$
$\bar{u}_k$	dimensionless coefficient $u_k h^k/U_o$
$\bar{x}$	dimensionless variable x/h
$\bar{y}$	dimensionless variable $yRe^{1/2}/h$
$\beta(\xi)$	function $\beta(\xi) = 2U'(x) \int_o^x U(x)dx/U^2(x)$
$\bar{\beta}_k$	dimensionless coefficient $\beta_k Re^k$
η	variable $\eta = U(x)y/\{2\nu\int_o^x U(x)dx\}^{1/2}$
$\bar{\eta}$	dimensionless variable $\bar{g}(\bar{x})\bar{y}$
ν	kinematic viscosity
ξ	variable $\xi = \frac{1}{\nu}\int_o^x U(x)dx$
$\bar{\xi}$	dimensionless variable ξ/Re

Symbols used by Witting in his finite difference method

A_r	$(r = 0,1 \ldots 5)$ constant coefficients
B_r	$(r = 0,1 \ldots 5)$ constant coefficients
h	dimension of lattice in x direction
i	position from starting point in x direction $(i = 0, \pm 1, \pm 2 \ldots h>0)$
k	position from plate surface in y direction $(k = 0, 1, 2 \ldots \ell>0)$

ℓ dimension of lattice in y direction

$L_{i,k}$ $\nabla_{i-1,0} - k/6\ (\nabla^2_{i+1,0} - \nabla^2_{i-1,0})$

$N_{i,k}$ see equation 81

p pressure

$S_{i,k}$ $\sum_{r=1}^{k-1} \Delta_{i,r}$

$u_{i,k}$ velocity component in x direction located by $u(x_i, y_k)$

$\hat{u}_i(y)$ polynomial approximation to velocity in vicinity of plate surface

$v_{i,k}$ velocity component in y direction located by $v(x_i, y_k)$

x_i x coordinate point at i th section

y_k y coordinate point at k th line above plate surface

$Z_{i,k}$ see equation 82

$\Delta_{i,k}$ $u_{i+1,k} - u_{i-1,k}$

$\nabla_{i,k}$ $u_{i,k+1} - u_{i,k-1}$

$\nabla^2_{i,k}$ $\nabla_{i,k+1} - \nabla_{i,k-1}$

ζ density

CHAPTER I

INTRODUCTION

The study of fluid flow separation has been an important area of fluid mechanic research for a number of years. Whenever a moving fluid is contained, there exists the possibility that at some point in the flow separation may occur. When this happens, the normal flow behavior breaks down and the flow can become erratic and unstable. The fluid flow parameter which is generally used to quantitatively describe this behavior is the wall shear stress. Where the wall shear stress equals zero, the flow is said to have separated at that point. This fluid flow behavior is common to a majority of fluid handling devices. Directly or indirectly flow separation leads to loss of efficiency in turbomachines, increased drag on submerged objects, generation of noise in flow processes, and alteration of heat transfer characteristics between fluid and solid boundaries.

Some of the earlier investigations into this general problem dealt with the flow separation from the downstream surface of an infinite cylinder. Schubaurer[2] presented an analytical solution for the separting laminar boundary layer of an infinite cylinder. Von Kármán and Millikan[1] presented a mathematical discussion of the boundary layer equations with the view of facilitating the investigation of separation. Nikuradse[3] has studied flow in variable wall two dimensional converging and diverging channels. Abramowitz[4] extended this configuration by considering the backflow resulting from diverging channels. Because of confusion in the meaning of the term separation, Maskell[5] has

defined the phenomenon in terms of a limiting streamline which lies infinitesimally close to the boundary surface before separation and "leaves" the surface at separation. With this definition it is possible to consider three dimensional separation in a broader and more meaningful sense.

The problem here is to study a two-dimensional steady laminar fluid flow which is directed into a two-dimensional corner. The flow direction is normal to the line of intersection of the two walls making up the corner. In particular, the aim will be to predict the separation point of the fluid flow along the wall section which is parallel to the flow direction. As the flow proceeds into the corner it moves against an increasing pressure. This adverse pressure gradient causes a thickening of the boundary layer and will eventually cause separation. The usual methods of predicting separation require a knowledge of the mainstream pressure gradient in advance. The attempt is made to eliminate this step for simple configurations.

In regard to problems of corner flow with incompressible fluids, work has been done for the case of the mainstream flow being parallel to the wall intersection. References 6, 7, 8, and 9 deal with the flow in straight and curved ducts. References 10, 11, 12, 13, and 14 are concerned with flow parallel to the intersection of two semi-infinite walls. However, with the exception of the case of flow in curved ducts, where secondary flow plays an important part, none of the above cases will result in flow separation.

There are two possible avenues of approach to the problem under study. The flow configuration and behavior is shown below. As the flow proceeds along the duct toward the corner, it engages the leading edge

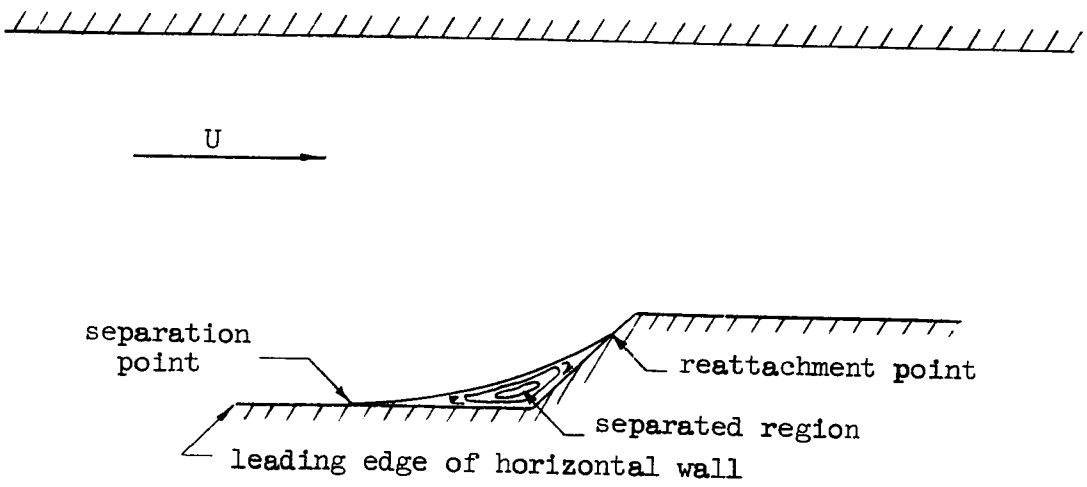

of the horizontal plate. The momentum change in the mainstream will be felt in the boundary layer which forms along the horizontal wall. The result is that the increasing pressure will cause a thickening of the boundary layer and separation results. The flow can be divided into two regimes - the outer flow where viscous action of the fluid flow is negligible, and the boundary layer and separated region where viscous action is very important. The outer flow moves over the horizontal plate and up and over the back wall. At the same time the fluid inside the boundary layer will decelerate and finally separate from the wall. The fluid inside the separated region will in general move in a vortex motion. This is experimentally verified by Reference 6 and the author's photographs (Figure 13). As mentioned, two approaches may be taken. One approach is to consider the outside flow and boundary layer as controlling the location of the separation point, and at the same time approximate the flow behavior inside the separated region so as to simplify the problem. Another approach is to try to describe the flow in the separated region and use this to predict the upstream separation point and the downstream

reattachment point. The latter approach could be attacked by considering that the separated region is filled with one steadily flowing vortex, as shown.

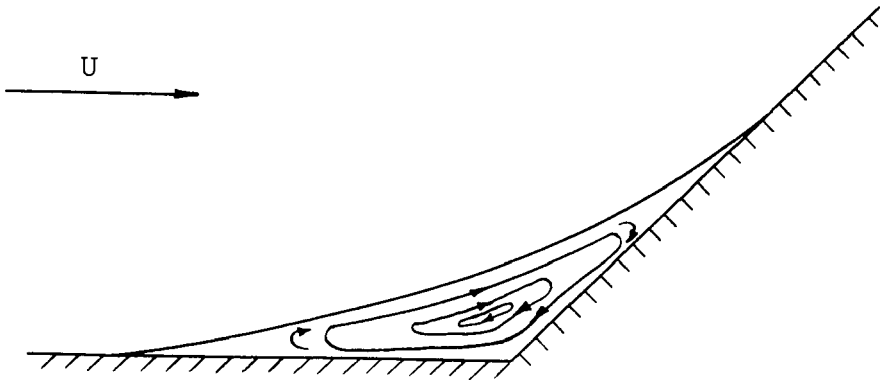

First the stream function for the vortex region must be found. This must then be matched to the outside flow by considering that the velocities along the separation line must be equal. Batchelor(15) has considered this general type of problem, where he shows that the closed streamlines for steady laminar flow at large Reynold's numbers must satisfy Poisson's equation. He points out the difficulty that Poisson's equation must be matched at one boundary to a streamline whose shape and velocity distribution are unknown. Second the rotational speed and size of the vortex region must be found. To do this the viscosity of the fluid must be taken into account. One approach would be to solve the boundary layer equations for the flow adjacent to the walls. This assumes that the boundary layer equations will describe the flow accurately which is very doubtful, especially in the vicinity of the corner. It would probably be more realistic in an analysis of this type to make only minor simplifications in the

Navier-Stokes equations. This would add considerably to the difficulty of the problem. Aside from the mathematical complexity of this approach there are other undesirable aspects from an engineering point of view. First, although the mainstream may be laminar and the boundary layer flow laminar to the point of separation, the separated region may have more than one vortex. This was noticed by the author during smoke visualization studies. This solution for a single vortex would then be limited to certain ranges of the laminar flow regime. Second, the solution based on the above analysis would be valid for only one configuration. It is desirous to obtain a solution which can be applied to a large number of configurations.

As mentioned there is another avenue of approach. This is to consider the outer flow and the boundary layer up to the point of separation. A potential solution for the flow outside the regions of viscous action is obtained. The resulting pressure distribution is then used in the boundary layer equations. Solving the boundary layer equations along the horizontal wall from the leading edge should give the separation point. One undesirable aspect is that in many cases potential solutions can be found for geometries which involve separation but the potential solution will not admit to a separation point. Then when the pressure distribution of the potential solution is fitted into the boundary layer equations, a separation point results. But this alters the flow so that the pressure distribution is changed. The results are an iteration scheme of some kind where separation is assumed and then must be checked. The problem which results is that the separation point must be known before it can be predicted.

The analysis which follows is of this general nature, but the separated region is defined beforehand and the iteration scheme is reduced to one step after the determination of the velocity of separation. The potential solution is a generalization of Lighthill's well known "flow up a step".(16) Lighthill considered an infinite fluid flowing over a 90° step. In order to quantitatively evaluate this flow he assumed that the flow inside the separated region is stagnant or at least at a velocity which is low compared to the outside flow. This means that the pressure inside the separated region is everywhere equal. Therefore, the velocity along the separating streamline, that is the streamline between the outer flow and the separated region, is constant. This allows a potential solution which can be obtained by means of conformal mapping techniques. In particular the solution is in a class of hydrodynamic problems called "free streamline solutions." However, as mentioned before, the potential solution will not admit to a separation point. Lighthill overcomes this very neatly. Referring to the following sketch it can be seen that the

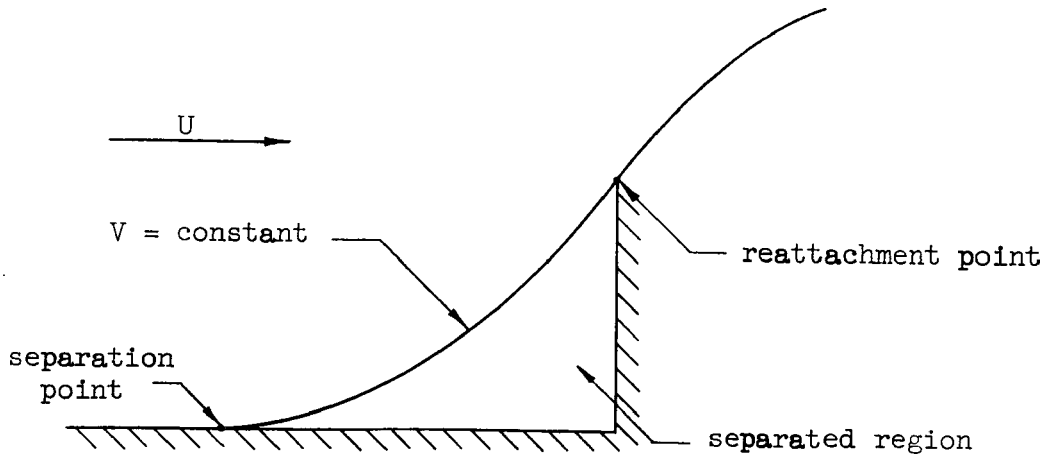

separated region can be defined by considering only the potential solution. However, the length of the horizontal wall from the leading edge to the separation point cannot be determined by inviscid flow theory alone. This is where viscous flow theory in the form of the boundary layer equations must enter. Lighthill defines this length by realizing that the velocity at the separation point must be a certain percentage of the velocity at the leading edge of the horizontal wall. Then he places the leading edge just far enough forward so that this velocity must occur at the separation point. As a result of this he completely defines the flow geometry. Now the velocity reduction from the leading edge to the separation point will be a function of the transition to turbulence of the boundary layer. If the boundary layer is laminar all the way, then one value of velocity reduction should result. If transition to turbulence occurs along the plate, then another value of velocity reduction will result. The case under study here is for a laminar boundary layer. In Lighthill's analysis he assumed a separation velocity for laminar flow. He checked this assumption against a photograph in Goldstein.[17]

It would seem that there are a great number of problems which can yet be evaluated with this approach. Thwaites[18] mentions this approach to these problems and also mentions the lack of work done in this area. Actually the general problem of defining a "separated" fluid by rigid walls and "free streamlines" was considered as long ago as 1914 by Villat.[19] He was followed by Thiry[20] and Odquist.[21] However, in each case they were confronted with a "mathematical indeterminacy"

to the problem. This means that mathematics alone could not produce a physical reality. Some of the geometries considered were physically impossible although mathematically realizable.

The study proposed here is in three parts:

(a) To generalize Lighthill's solution by considering a finite fluid which moves against an obstacle which is at any angle between 0° and 90° to the horizontal. Also the solution is generalized by assuming that reattachment takes place along the obstacle's forward face. Lighthill assumes reattachment only at the top of the obstacle which is always at 90° to the horizontal. As will be shown the solution under study here will include Lighthill's solution when his geometry is assumed.

(b) To verify the assumed velocity of separation by means of the boundary layer equations. Görtler's series solution of the boundary layer equations along with Witting's finite difference solution (which are particularly applicable in this case) are employed.

(c) To experimentally evaluate the entire approach to this problem. A steady laminar flow of air was used for this. Static pressure measurements as well as visualization techniques were used.

CHAPTER II

POTENTIAL FLOW SOLUTION FOR EXTERNAL FLOW

A. Mathematical Solution

As previously mentioned the physical simplification in the approach outlined is to assume that within the separated region the flow is stagnant. The general flow geometry is as shown:

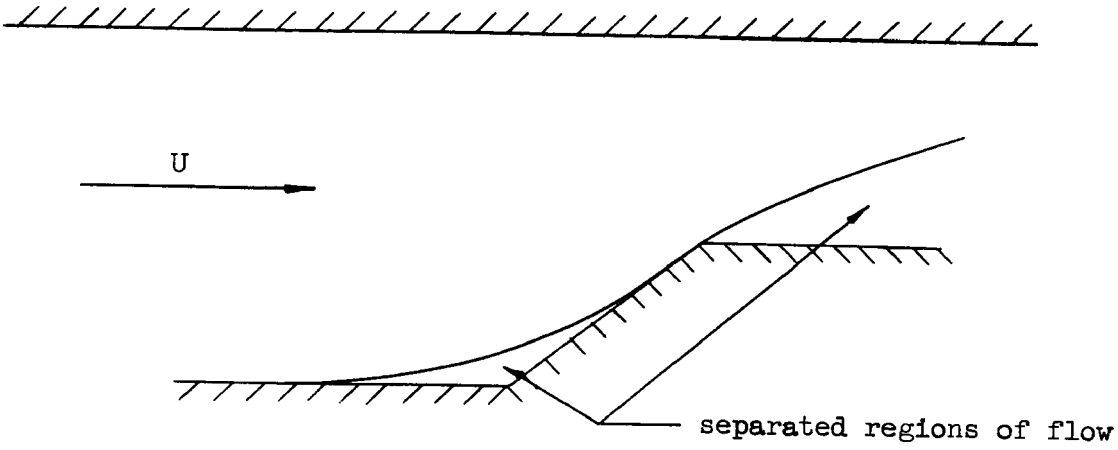

The fluid flows into the corner and engages the leading edge of the horizontal plate. The resulting momentum change causes the flow to separate. There are actually two separated regions of flow. One region is in the corner and the other is at the top of the back wall where the momentum of the flow will not allow the fluid to break sharply around the corner. The potential flow solution is set up as follows:

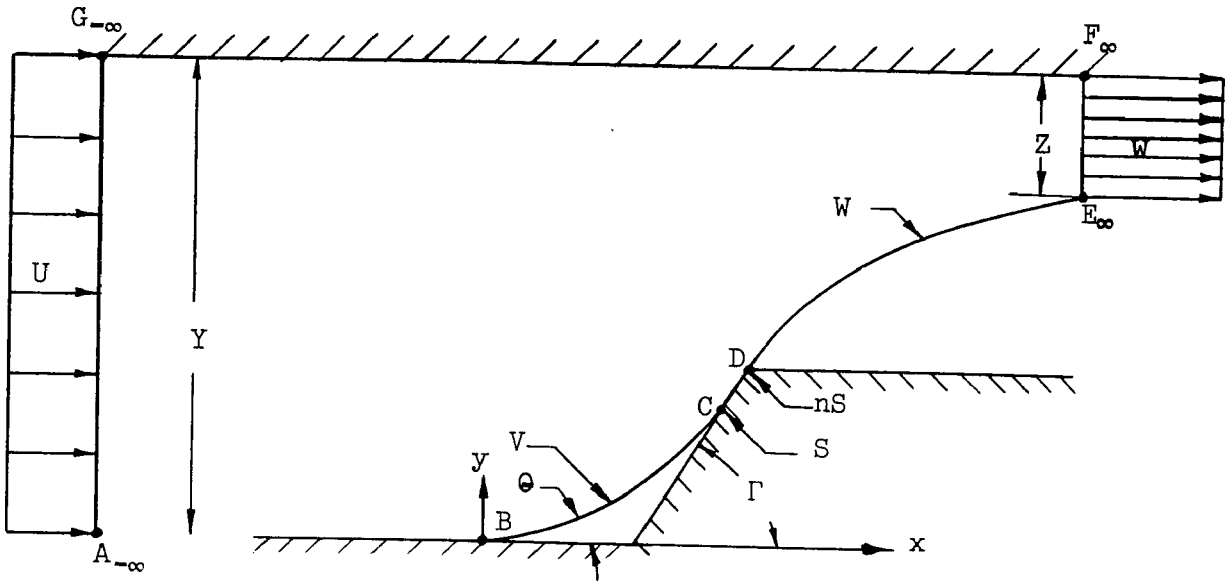

Potential flow theory predicts that any disturbance to the flow will be felt infinitely far in any direction. In this case it means that the disturbance of the obstacle will be felt infinitely far upstream and downstream. Placing the x-y origin at point B, as shown, requires that the uniform velocity U of the incoming flow be infinitely far upstream. As the flow progresses from point A to point B along the line A-B, a deceleration will take place. Some place between A and B the flow will engage the leading edge of the horizontal plate. Separation occurs at point B. Along the line B-C the velocity is constant and equal to V. The velocity V must be less than U since the pressure at B is greater than the pressure at A. The line B-C is commonly referred to as a "free streamline." The distance from point B to point C is denoted by S. The angle at any point of the line B-C with the horizontal is denoted by Θ.

At point C the flow reattaches to the back wall. The back wall is at an angle Γ with the horizontal. The distance from point B

to point D along the line B-C-D is denoted by nS. Therefore n is only a multiple of S and must be greater than unity. At point D the flow again separates from the surface of the duct and another area of stagnant flow is assumed between the line D-E and the lower horizontal wall. Now this disturbance must be felt infinitely far downstream to a point where the velocity is uniform and equal to W. The line D-E is also a "free streamline" along which the velocity is constant and equal to W. The channel depth is denoted by Y and the distance between the free streamline at point E and the top of the channel is Z. Continuity then says that UY = WZ. It is assumed that the free streamline B-C is tangent to the wall at points B and C.

The complex potential is defined as $w = \phi + i\psi$, where ϕ is the potential function and ψ is the stream function. Then if $\psi = 0$ along the line A-B-C-D-E and $\phi = 0$ through the point B, the flow in the w plane would be represented as follows:

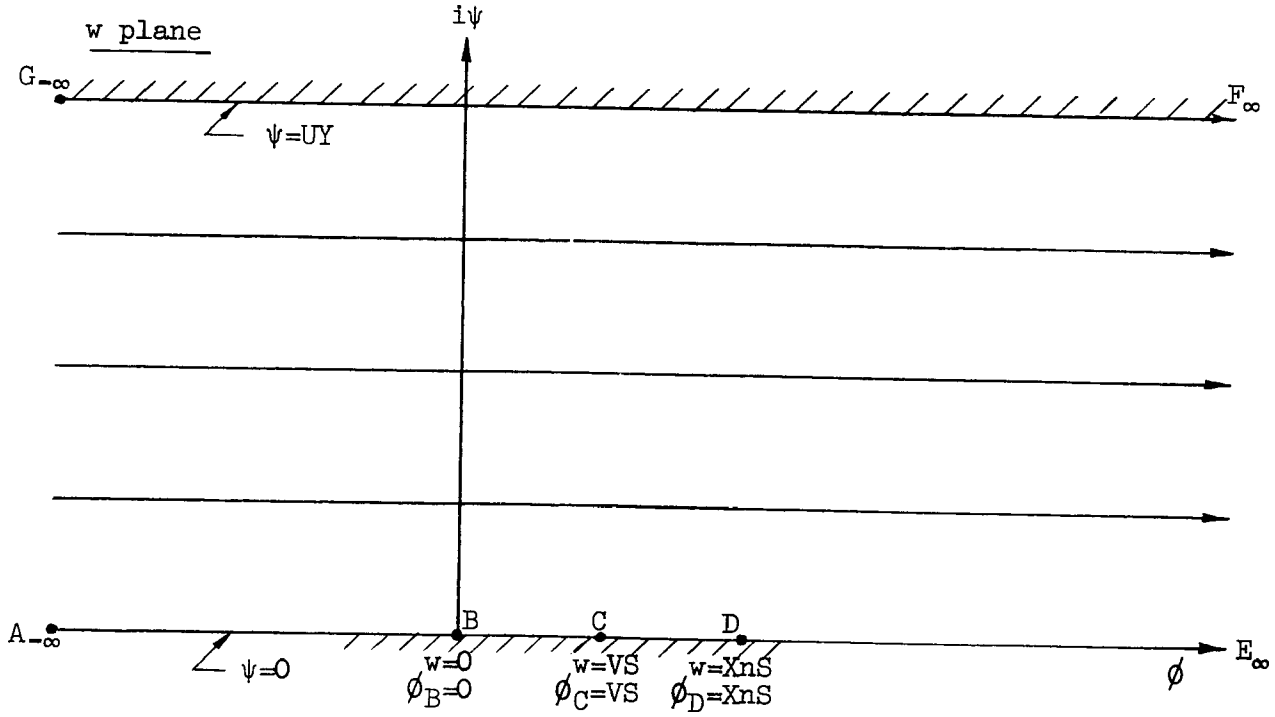

Since along $\psi = 0$, $w = \phi$ then at point B $\phi_B = 0$. Also $\frac{\partial \phi}{\partial s} = q$ where q is the velocity in the direction of s. Therefore, along the line B-C

$$\int_{\phi=0}^{\phi=\phi_c} d\phi = \int_{s=0}^{s=S} q\,ds \quad , \qquad \text{but} \qquad q = V$$

Then it follows from this that

$$\phi_c = VS \tag{1}$$

Using the same analysis for point D we can get

$$\int_{\phi=0}^{\phi=\phi_D} d\phi = \int_{s=0}^{s=nS} q\,ds$$

Here, however, q is not constant over the entire length but varies along C-D. To simplify matters, let $XnS = \int_0^{nS} qds$, where obviously

$$X = \frac{\int_0^{nS} q\,ds}{nS} \tag{2}$$

The next transformation involves the complex velocity dw/dz and is

$$\Omega = \ln \frac{dw}{dz} = \ln q e^{-i\theta} \tag{3}$$

where $qe^{-i\theta}$ is the complex velocity. Therefore,

$$\ln \frac{dw}{dz} = \ln q e^{-i\theta} = \ln q - i\theta \qquad \text{and}$$

$$\Omega = \ln q - i\theta \tag{4}$$

The mapping of the z plane to the Ω plane is shown below.

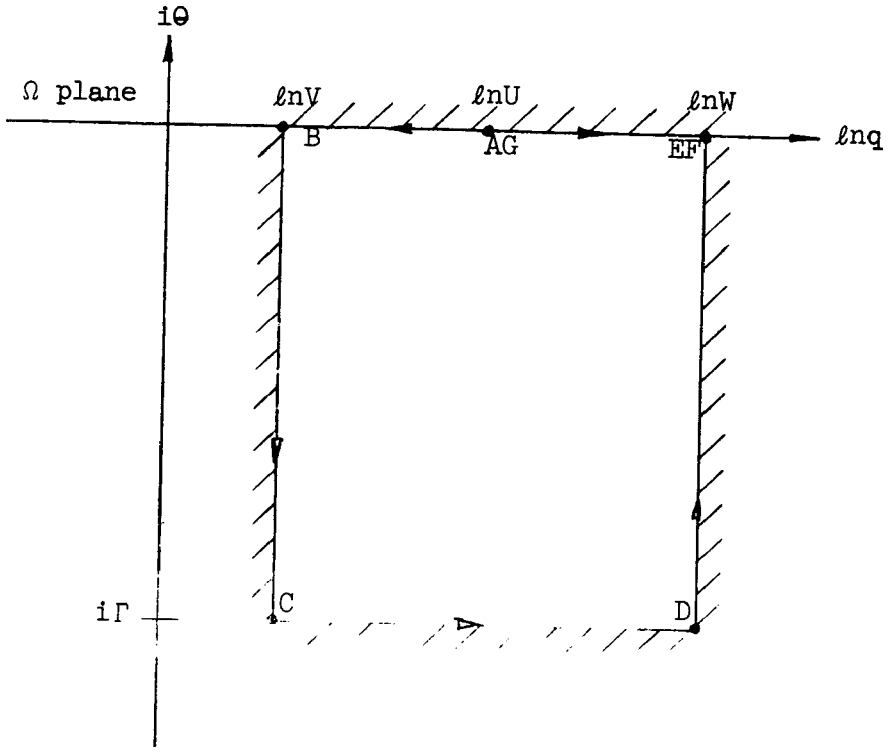

Ultimately, it is desired to transform the above rectangle into the upper half plane. But first it is required that the w plane be transformed into the upper half plane. For this the Schwarz-Christoffel transformation gives

$$w = \frac{UY}{\pi} \ell n\, t \qquad (5)$$

The mapping in the t plane is as shown:

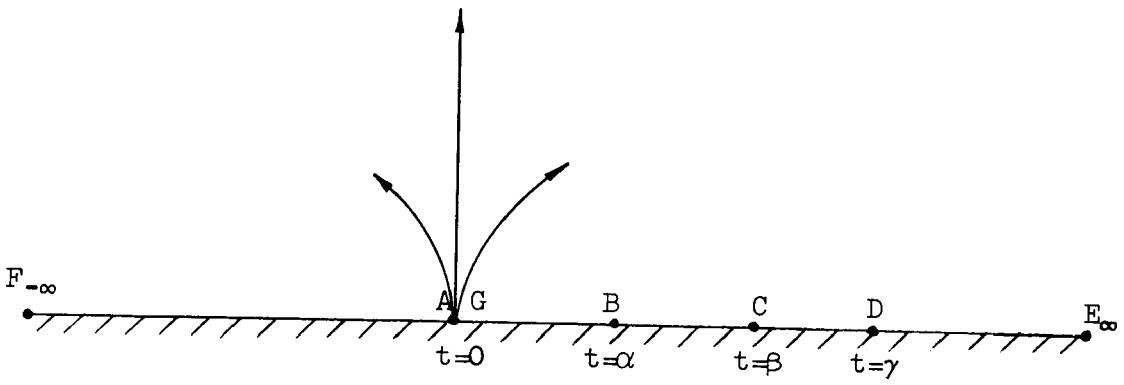

Finally, what is needed is to find the transformation between the t plane and the Ω plane. With this transformation there can ultimately be obtained a relationship between velocity and coordinate position.

The transformation from the t-plane and the Ω plane, is made by means of the Schwarz-Christoffel transformation. The result is

$$\Omega = \bar{L} \int \frac{dt}{(AG-t)^{\lambda/\pi}(B-t)^{\mu/\pi}(C-t)^{\eta/\pi}(D-t)^{\epsilon/\pi}} + \bar{K} \qquad (6)$$

where by referring to the t-plane

$$AG=0 \ , \quad B=\alpha \ , \quad C=\beta \ , \quad \text{and} \quad D=\gamma$$

Referring to the Ω plane $\lambda = 0$, $\mu = \pi/2$, $\eta = \pi/2$, $\epsilon = \pi/2$ and (5) becomes

$$\Omega = \bar{L} \int \frac{dt}{[(\alpha-t)(\beta-t)(\gamma-t)]^{1/2}} + \bar{K} \qquad (7)$$

Now returning to the w plane and the t-plane it can be seen that

at point B $w = 0$, $t = \alpha$

at point C $w = VS$, $t = \beta$

and at point D $w = XnS$, $t = \gamma$.

Then using the transformation $w = \frac{UY}{\pi} \ell nt$ for point B

$0 = \frac{UY}{\pi} \ell n\alpha$ and α must equal one.

For point C

$$VS = \frac{UY}{\pi} \ell n\beta \quad , \quad \text{so that}$$

$$\beta = \exp\left(\frac{\pi VS}{UY}\right) \tag{8}$$

For point D

$$XnS = \frac{UY}{\pi} \ell n\gamma \quad , \quad \text{so that}$$

$$\gamma = \exp\left(\frac{n\pi XS}{UY}\right) \tag{9}$$

Then

$$\Omega = \bar{L} \int \frac{dt}{[(1-t)(\beta-t)(\gamma-t)]^{1/2}} + \bar{K} \tag{10}$$

Next the integral $\int \frac{dt}{[(1-t)(\beta-t)(\gamma-t)]^{1/2}}$ must be solved.

First

$$\int \frac{dt}{[(1-t)(\beta-t)(\gamma-t)]^{1/2}} = \frac{+}{-} \frac{1}{i} \int \frac{dt}{[(t-1)(\beta-t)(\gamma-t)]^{1/2}}$$

Let

$$(t-1)^{1/2} = x'$$

then

$$x'^2 = t-1$$

or

$$x'^2+1 = t$$

so that

$$2x'dx' = dt \, .$$

Then

$$\pm\frac{1}{i}\int\frac{dt}{[(t-1)(\beta-t)(\gamma-t)]^{1/2}} = \pm\frac{1}{i}\int\frac{2x'dx'}{x'[(\beta-x'^2-1)(\gamma-x'^2-1)]^{1/2}}$$

$$= \pm\frac{2}{i}\int\frac{dx'}{[(\beta-x'^2-1)(\gamma-x'^2-1)]^{1/2}}$$

Let $N = \beta-1$ and $M = \gamma-1$ and also let $x' = \sqrt{N}\sin\theta'$ where θ' is a new variable. Then

$$\theta' = \sin^{-1}\frac{x'}{\sqrt{N}} = \sin^{-1}\sqrt{\frac{t-1}{N}} \qquad (11)$$

$x'^2 = N\sin^2\theta'$ and therefore $N-x'^2 = N(1-\sin^2\theta') = N\cos^2\theta'$

$dx' = \sqrt{N}\cos\theta' d\theta'$

Then

$$\pm\frac{2}{i}\int\frac{dx'}{[(N-x'^2)(M-x'^2)]^{1/2}} = \pm\frac{2}{i\sqrt{M}}\int\frac{d\theta'}{[1-\frac{N}{M}\sin^2\theta']^{1/2}}$$

so that the transformation becomes:

$$\Omega = \pm\frac{2\bar{L}}{i\sqrt{M}}\int\frac{d\theta'}{[1-\frac{N}{M}\sin^2\theta']^{1/2}} + \bar{K} \qquad (12)$$

Now

$$\int\frac{d\theta'}{[1-k^2\sin^2\theta']^{1/2}}$$

is the usual elliptic integral of the first kind. The parameter k is called the modulus and is equal to $\sqrt{\frac{N}{M}}$ for this case. Using the inverse

Jacobian elliptic functions the above can be written:

$$\int \frac{d\theta'}{[1-k^2\sin^2\theta']^{1/2}} = sn^{-1}\left(\sqrt{\frac{t-1}{N}}, k\right) \qquad (13)$$

(c.f. references 22, 23, and 24).

Then the transformation becomes

$$\Omega = \pm \frac{2\bar{L}}{i\sqrt{M}}\, sn^{-1}\left(\sqrt{\frac{t-1}{N}}, k\right) + \bar{K} \qquad (14)$$

The next step is to evaluate the constants of integration $\bar{L}$ and $\bar{K}$. To evaluate $\bar{K}$ point B may be used. At point B

$$w=0\ ,\ t=1\ ,\ \Omega = \ln V \quad \text{since} \quad \theta=0\ .$$

Therefore $\ell nV = \bar{K}$ because $sn^{-1}(0,k) = 0$.

To evaluate $\bar{L}$ point A is used. At point A

$$w=-\infty\ ,\ t=0\ ,\ \Omega = \ln U \quad \text{since} \quad \theta=0\ .$$

Therefore,

$$\ln U/V = \pm \frac{2\bar{L}}{i\sqrt{M}}\, sn^{-1}\left(\sqrt{-\frac{1}{N}}, k\right) \qquad (15)$$

Let

$$\frac{i\sqrt{M}\ln U/V}{2\bar{L}} = iy'\ ,$$

then

$$sn(iy', k) = i\sqrt{\frac{1}{N}}$$

where the positive root of (15) is used.

Using Reference 22

$$sn(iy; k) = i\,tn(y; k') \quad . \tag{16}$$

k' is the complementary modulus and is given by

$$k' = \sqrt{1 - k^2} \quad . \tag{17}$$

Using (16)

$$i\,tn(y; k') = i\sqrt{\frac{1}{N}}$$

and

$$\frac{\sqrt{M}\ln U/V}{2\bar{L}} = tn^{-1}\left(\sqrt{\frac{1}{N}}, k'\right) \tag{18}$$

or

$$\frac{2\bar{L}}{\sqrt{M}} = \frac{\ln U/V}{tn^{-1}\left(\sqrt{\frac{1}{N}}, k'\right)} \tag{19}$$

Therefore, both constants have been evaluated and finally there is

$$i(\Omega - \ln V) = \frac{\ln U/V}{tn^{-1}\left(\sqrt{\frac{1}{N}}, k'\right)}\, sn^{-1}\left(\sqrt{\frac{t-1}{N}}, k\right) \tag{20}$$

For simplicity let

$$P = \frac{tn^{-1}\left(\sqrt{\frac{1}{N}}, k'\right)}{\ln U/V} \tag{21}$$

so that

$$iP(\Omega - \ln V) = sn^{-1}\left(\sqrt{\frac{t-1}{N}}, k\right) \tag{22}$$

where

$$K = \sqrt{\frac{N}{M}} \tag{23}$$

$$N = \beta - 1 = \exp\left(\pi \frac{Y}{U} \frac{S}{Y}\right) - 1 \tag{24}$$

$$M = \gamma - 1 = \exp\left(\pi n \frac{X}{U} \frac{S}{Y}\right) - 1 \tag{25}$$

and

$$t = \exp\left(\frac{\pi w}{UY}\right) \tag{26}$$

(22) is then the general relationship between the Ω plane and the t plane.

So far we have used points A and B to determine the constants $\bar{L}$ and $\bar{K}$. Points C and D can also be used to determine some further properties of the flow.

At point C

$$\Omega = \ln V - i\Gamma$$

$$w = VS \quad \text{and} \quad t - 1 = N$$

When these are substituted into (22), there results

$$iP(-i\Gamma) = sn^{-1}(1, k) \quad \text{or}$$

$$P\Gamma = K \tag{27}$$

K is the complete elliptic integral, or

$$K = \int_0^{\pi/2} \frac{d\theta'}{\sqrt{1 - k^2 \sin^2\theta'}}$$

At point D

$$\Omega = \ln W - i\Gamma$$

$$w = \mathrm{sn}\, S$$

$$t - 1 = M$$

When these are substituted into (22), then

$$iP\left(\ln \frac{W}{V} - i\Gamma\right) = \mathrm{sn}^{-1}\left(\sqrt{\frac{M}{N}}, \sqrt{\frac{N}{M}}\right)$$

$$iP \ln \frac{W}{V} + P\Gamma = \mathrm{sn}^{-1}\left(\frac{1}{k}, k\right) \tag{28}$$

Reference 22 shows that

$$\mathrm{sn}^{-1}\left(\frac{1}{k}, k\right) = K + iK'$$

where K' is the complete elliptic integral when k' is the modulus, or $K' = K(k')$.

Then

$$iP \ln \frac{W}{V} + P\Gamma = K + iK'$$

and equating real and imaginary parts, there results as before

$$P\Gamma = K$$

and

$$P \ln \frac{W}{V} = K' \tag{29}$$

At point E

$$\Omega = \ln W$$

$$w = \infty$$

$$t - 1 = \infty$$

and (22) becomes

$$i P \ln W/V = sn^{-1}(\infty, k) = iK' ,$$

so that as before

$$P \ln W/V = K'$$

Equation (29) gives a further restriction on the flow.

Now returning to the x-y plane, it is necessary to calculate the distances c, b, a, and h in order to determine the geometry of the flow.

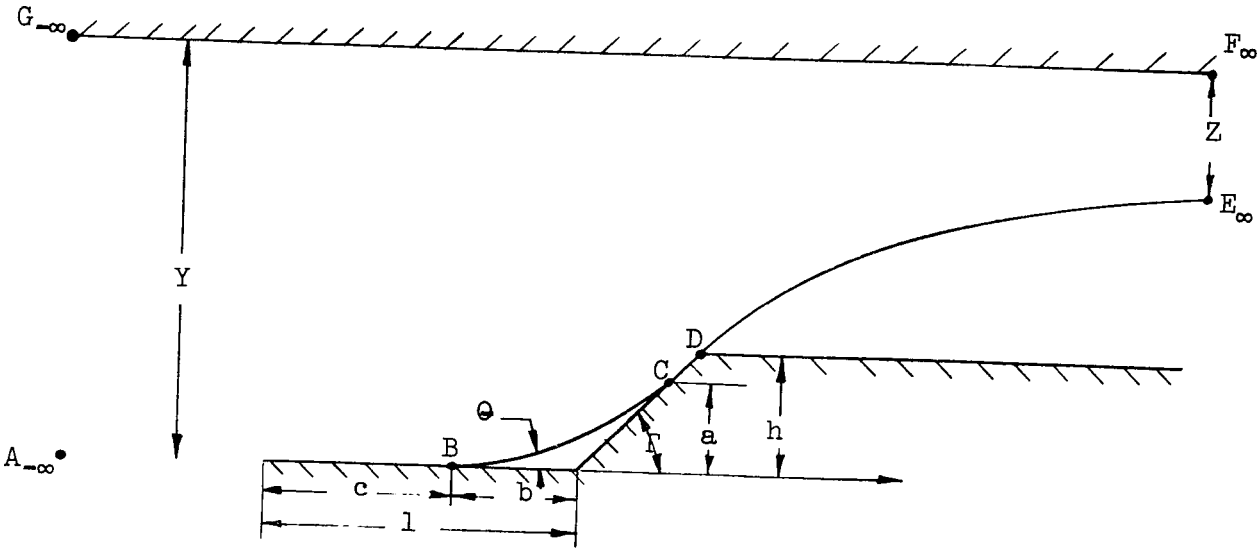

The first step in this direction is to obtain the equation of the line B-C. Along the line B-C, $w = Vs$, where s is the distance along line B-C measured from point B. Since along this line $\psi = 0$, then $\phi = Vs$. Then $t = \exp(\frac{\pi Vs}{UY})$ and $\Omega = \ell nV - i\Theta$ where Θ is the angle that the line B-C makes with the horizontal. Using these in (22) gives

$$iP(\ln V - i\theta - \ln V) = sn^{-1}\left(\sqrt{\frac{t-1}{N}}, k\right)$$

or

$$sn^2(P\theta, k) = \frac{\exp(\frac{\pi V}{U}\frac{s}{Y}) - 1}{N} \qquad (30)$$

Equation (30) can be expressed as

$$\frac{s}{Y} = \frac{U}{\pi V} \ln\left[N\,sn^2(P\theta, k) + 1\right] \tag{31}$$

In order to obtain an equation for curve B-C in terms of the x-y coordinates one notes that

$$dx = \cos\theta\, ds \quad , \quad dy = \sin\theta\, ds$$

hence (31) can be written

$$\frac{dx}{Y} = \cos\theta\,\frac{ds}{Y} = \cos\theta\,\frac{U}{\pi V}\, d\left\{\ln\left[N\,sn^2(P\theta, k) + 1\right]\right\}$$

$$\frac{dy}{Y} = \sin\theta\,\frac{ds}{Y} = \sin\theta\,\frac{U}{\pi V}\, d\left\{\ln\left[N\,sn^2(P\theta, k) + 1\right]\right\}$$

Therefore, the coordinate position of any point on the line B-C can be given by

$$\frac{x}{Y} = \frac{U}{\pi V}\int_0^{\theta} \cos\theta\, d\left\{\ln\left[N\,sn^2(P\theta, k) + 1\right]\right\} \tag{32}$$

$$\frac{y}{Y} = \frac{U}{\pi V}\int_0^{\theta} \sin\theta\, d\left\{\ln\left[N\,sn^2(P\theta, k) + 1\right]\right\} \tag{33}$$

(32) and (33) can be solved to give the shape of the "free streamline" B-C. Also when $\theta = \Gamma$, the angle of the obstacle, then $\frac{x}{Y} = \frac{b}{Y} + \frac{a}{Y}\cot\Gamma$ and $\frac{y}{Y} = \frac{a}{Y}$, so that

$$\frac{b}{Y} + \frac{a}{Y}\cot\Gamma = \frac{U}{\pi V}\int_0^{\Gamma} \cos\theta\, d\left\{\ln\left[N\,sn^2(P\theta, k) + 1\right]\right\} \tag{34}$$

$$\frac{q}{V} = \frac{U}{\pi V} \int_0^{\Gamma} \sin\theta \, d\{\ln[N\,sn^2(P\theta, k)+1]\} \qquad (35)$$

The author could not find a closed form expression for the integrals in (34) and (35); however, they were numerically evaluated using Simpson's Rule.

The next step is to find the length of plate from the leading edge to the separation point. To do this it is necessary to assume a velocity at point B which is a certain percentage of the velocity at the leading edge of the plate. This assumption must be checked by using viscous flow theory, but this will be discussed later. The leading edge is placed just far enough forward to cause a separation at point B. It is necessary then to obtain the relationship between the velocity of flow and the distance forward from point B.

From point B forward $\Omega = \ell nq$ where q is the velocity magnitude and $\Theta = 0$ from A to B.

Then (22) will give

$$iP(\ln q - \ln V) = sn^{-1}\left(\sqrt{\tfrac{\epsilon-1}{N}}, k\right)$$

$$iP(\ln q/V) = sn^{-1}\left(\sqrt{\tfrac{\epsilon-1}{N}}, k\right)$$

Using (16)

$$sn(iP \ln q/V, k) = i\,tn(P \ln q/V, k')$$

so that

$$sn^2(iP \ln q/V, k) = -tn^2(P \ln q/V, k')$$

Let $z' = \ell n\ q/V$, then

$$\exp\left(\frac{\pi w}{UY}\right) = -N tn^2(P_3', k') + 1$$

and

$$w = \frac{UY}{\pi} \ell n\left[-N tn^2(P_3', k') + 1\right] \tag{36}$$

Since $w = \phi + i\psi$ and from A to B $\psi = 0$, then

$$\phi = \frac{UY}{\pi} \ell n\left[-N tn^2(P_3', k') + 1\right] \tag{37}$$

Since $q = \frac{\partial \phi}{\partial s}$ then $d\phi = q\,ds$. Along A-B $ds = dx$, so that

$$\frac{dx}{Y} = \frac{U}{\pi V} \frac{V}{q} d\left\{\ell n\left[-N tn^2(P_3', k') + 1\right]\right\} \tag{38}$$

Since $q/V = e^{z'}$, then $V/q = e^{-z'}$ so that

$$\frac{dx}{Y} = \frac{U}{\pi V} e^{-\beta'} d\left\{\ell n\left[-N tn^2(P_3', k') + 1\right]\right\}$$

Integrating then gives:

$$\frac{x}{Y} = \frac{U}{\pi V} \int_0^{\beta'} e^{-\beta} d\left\{\ell n\left[-N tn^2(P_3', k') + 1\right]\right\} \tag{39}$$

Now the upper limit of the integral will determine the value of $\frac{x}{Y}$; and since $z' = \ell n\ q/V$, then the velocity of the flow is determined. The value of q/V varies from unity at the separation point to the value of U/V at point A. $\frac{c}{Y}$ is determined as equal to $-\frac{x}{Y}$ when

q/V is picked at the leading edge of horizontal plate. When q/V is divided by the value of q/V at the leading edge, this ratio becomes the separation velocity at the separation point.

In order to complete the solution it is necessary to find the distance h. Presently a/Y has been determined. If the distance between points C and D can be found then h/Y can be determined. This distance is determined, obviously, by consideration of the flow from point C to point D. Along this line

$$\Omega = \ln q - i\Gamma$$

and therefore (22) gives

$$iP[\ln q/V - i\Gamma] = sn^{-1}\left(\sqrt{\frac{t-1}{N}}, k\right)$$

$$iP \ln q/V + P\Gamma = sn^{-1}\left(\sqrt{\frac{t-1}{N}}, k\right)$$

Equation (27) gives $P\Gamma = K$ so that

$$iP \ln q/V + K = sn^{-1}\left(\sqrt{\frac{t-1}{N}}, k\right)$$

or

$$sn\left(iP \ln q/V + K, k\right) = \sqrt{\frac{t-1}{N}}$$

Reference (23) shows that

$$sn\left(K + iP \ln q/V, k\right) = \frac{1}{dn\left(P \ln q/V, k'\right)}$$

so that

$$\sqrt{\frac{t-1}{N}} = \frac{1}{dn\left(P \ln q/V, k'\right)} \qquad (40)$$

Again let $\ell n\ q/V = z'$, then Equation (40) can be written

$$t = \frac{N}{dn^2\left(Pz', k'\right)} + 1$$

where

$$t = \exp\left(\frac{\pi w}{UY}\right)$$

so that

$$w = \frac{UY}{\pi} \ln\left\{\frac{N}{dn^2(P_{z'}, k')} + 1\right\} \tag{41}$$

Along C-D

$$\phi = \frac{UY}{\pi} \ln\left\{\frac{N}{dn^2(P_{z'}, k')} + 1\right\}$$

so that

$$ds = \frac{UY}{\pi q} d\left\{\ln\left[\frac{N}{dn^2(P_{z'}, k')} + 1\right]\right\}$$

Now this can be rearranged to give

$$\frac{ds}{Y} = \frac{U}{\pi V} \frac{V}{q} d\left\{\ln\left[\frac{N}{dn^2(P_{z'}, k')} + 1\right]\right\}$$

And since $z' = \ln q/V$ then

$$\frac{ds}{Y} = \frac{U}{\pi V} e^{-z'} d\left\{\ln\left[\frac{N}{dn^2(P_{z'}, k')} + 1\right]\right\} \tag{42}$$

Equation (42) must be integrated from $s = S$, where $q = V$ to $s = nS$ where $q = W$.

$$\int_S^{nS} \frac{ds}{Y} = \frac{U}{\pi V} \int_{z'=\ln V/V}^{z'=\ln W/V} e^{-z'} d\left\{\ln\left[\frac{N}{dn^2(P_{z'}, k')} + 1\right]\right\}$$

and gives

$$(n-1)\frac{S}{Y} = \frac{U}{\pi V} \int_0^{K'/P} e^{-z'} d\left\{\ln\left[\frac{N}{dn^2(P_{z'}, k')} + 1\right]\right\} \tag{43}$$

Equation (43) then completes the solution and allows the entire geometry of the flow to be determined. The solution is awkward in that it would be more useful if one could start with the geometry of the flow and then proceed to find the separation point. However, it is necessary to start with certain flow parameters and then determine the flow geometry.

At this point it is convenient to list the important relations that will be used for the solution. Summarizing then, the following will be important:

$$P = \frac{tn^{-1}\left(\sqrt{\frac{1}{N}}, k'\right)}{\ln U/V} \tag{21}$$

$$N = \exp\left(\frac{\pi V}{U}\frac{S}{Y}\right) - 1 \tag{24}$$

$$M = \exp\left(\pi n \frac{X}{U}\frac{S}{Y}\right) - 1 \tag{25}$$

$$k = \sqrt{\frac{N}{M}} \tag{23}$$

$$\Gamma = K/P \tag{27}$$

$$\ln W/V = K'/P \tag{29}$$

$$\frac{x}{Y} = \frac{U}{\pi V}\int_0^{\beta'} e^{-\beta'}\, d\left\{\ln\left[-N\,tn^2(P\beta', k') + 1\right]\right\} \tag{39}$$

$$\frac{b}{Y} + \frac{a}{Y}\cot\Gamma = \frac{U}{\pi V}\int_0^{\Gamma} \cos\theta\, d\left\{\ln\left[N\,sn^2(P\theta, k) + 1\right]\right\} \tag{34}$$

$$\frac{q}{V} = \frac{U}{\pi V} \int_0^{\pi} \sin\theta \, d\left\{ \ln\left[N \, sn^2(P\theta, k) + 1 \right] \right\} \qquad (35)$$

$$(n-1)\frac{S}{Y} = \frac{U}{\pi V} \int_0^{K'/P} e^{-\beta'} \, d\left\{ \ln\left[\frac{N}{dn^2(P\beta', k')} + 1 \right] \right\} \qquad (43)$$

B. Calculation of Lighthill's Solution

The solution of Reference 16 will be examined in the light of this analysis. Lighthill considers the case of an infinite fluid flowing over a 90° step. He also assumes reattachment at the top of the step or obstacle. This means that n = 1 in the above solution. From Equation (2) and n = 1

$$X = \frac{\int_0^S q \, ds}{S}$$

But from 0 to S q is constant and equal to V. Therefore, X = V. Then

$$N = \exp\left(\pi \frac{V}{U} \frac{S}{Y}\right) - 1$$

and

$$M = \exp\left(\pi \frac{V}{U} \frac{S}{Y}\right) - 1$$

so that k = 1. Reference 22 shows that sn(u,1) = tanh u. It is interesting to note at this point that when the modulus k goes to zero, the elliptic functions degenerate to the circular functions. When the modulus k goes to unity the elliptic functions reduce to the hyperbolic functions. Also, k must vary between zero and one.

Then with $k = 1$, $k' = 0$, so that $tn^{-1}(u,0) = \tan^{-1}u$ and

$$P = \frac{\tan^{-1}\sqrt{\frac{1}{N}}}{\ln U/V} \tag{44}$$

$K(0) = \pi/2$ and $K(1) = \infty$ so that $\Gamma P = \infty$ and $P \ln W/V = \pi/2$.

Then (39) becomes

$$\frac{X}{Y} = \frac{U}{\pi V}\int_0^{\beta'} e^{-\beta'} d\left\{\ln\left[-N\tan^2(P\beta')+1\right]\right\} \tag{45}$$

(34) and (35) are

$$\frac{b}{Y} + \frac{h}{Y}\cot\Gamma = \frac{U}{\pi V}\int_0^{\Gamma}\cos\theta\, d\left\{\ln\left[N\tanh^2(P\theta)+1\right]\right\} \tag{46}$$

$$\frac{h}{Y} = \frac{U}{\pi V}\int_0^{\Gamma}\sin\theta\, d\left\{\ln\left[N\tanh^2(P\theta)+1\right]\right\} \tag{47}$$

Equation (43) equals zero as $dn(u,0) = 1$ and therefore $\ell n(N+1) = \pi \frac{V}{U}\frac{S}{Y}$ which is a constant.

Equation (22) becomes

$$i\,P(\Omega - \ln V) = \tanh^{-1}\left(\sqrt{\frac{t-1}{N}}\right) \tag{48}$$

Next consider $Y \to \infty$. This means that $Z/Y \to 1$ and $W \to U$. In the w plane the streamline $\psi = UY$ goes to infinity so that the w plane becomes the t plane and the transformation $w = \frac{UY}{\pi}\ \ell n\ t$ is eliminated.

Another approach is to consider Equation (48). Take $\frac{t-1}{N}$ and let Y approach infinity. Then

$$\lim_{Y\to\infty} \frac{t-1}{N} = \lim_{Y\to\infty} \left\{ \frac{\exp\left(\frac{\pi w}{UY}\right) - 1}{\exp\left(\frac{\pi VS}{UY}\right) - 1} \right\} = \lim_{Y\to\infty} \left\{ \frac{\frac{-\pi w}{UY^2}}{\frac{-\pi VS}{UY^2}} \cdot \frac{\exp\left(\frac{\pi w}{UY}\right)}{\exp\left(\frac{\pi VS}{UY}\right)} \right\}$$

$$= \frac{w}{VS}$$

Therefore (48) becomes

$$i P(\Omega - \ln V) = \tanh^{-1}\sqrt{\frac{w}{VS}} \qquad (49)$$

where

$$P = \frac{\pi/2}{\ln U/V} \qquad (50)$$

This is the result obtained by Lighthill. From Equation (49) it is possible to get

$$\frac{b}{S} = \int_0^{\Gamma} \cos\theta \, d\left\{\tanh^2(P\theta)\right\} \qquad (51)$$

$$\frac{h}{S} = \int_0^{\Gamma} \sin\theta \, d\left\{\tanh^2(P\theta)\right\} \qquad (52)$$

and ahead of point B,

$$\frac{X}{S} = -\int_0^{\beta'} e^{-\beta'} d\left\{\tan^2(P\beta')\right\} \qquad (53)$$

C. Scheme of Calculation

Returning to the general solution, the following steps are presented as a logical scheme of calculation.

(1) Select the parameters U/V, S/Y, and the modulus k. Although the effects of each parameter are interwoven, U/V is the primary factor in controlling the dimensionless length, $1/Y$. S/Y will control the channel depth to step height; and k has a large effect on the angle of the obstacle. The reason for choosing k is that most tables of elliptic functions are set up on the basis $\sin^{-1}k$. This eliminates a great deal of interpolation.

(2) Having selected k, then k', K, and K' are determined.

(3) Calculate $\ell n\ U/V$ and N

(4) Calculate $M = N/k^2$

(5) Calculate $P = \dfrac{tn^{-1}(\sqrt{\frac{1}{N}},\ k')}{\ell n\ U/V}$

(6) Then the angle of the obstacle is determined from $\Gamma = K/P$

(7) Calculate $\ell n\ W/V = K'/P$ and since $W/V = \frac{U}{V}\ \frac{Y}{Z}$ then calculate

$$Y/Z = V/U\ e^{K'/P} \qquad (54)$$

Equation (54) will give some idea of the channel height to obstacle height to be expected.

(8) Next evaluate (43). This will give n.

(9) If desired $\frac{X}{U}$ may be evaluated by use of (25).

(10) By evaluating (34), (35) and (39), $\frac{b}{Y}$, $\frac{a}{Y}$, and $\frac{c}{Y}$ can be obtained.

(11) Then $\frac{\ell}{Y} = \frac{c}{Y} + \frac{b}{Y}$ and

(12) $\frac{h}{Y} = \frac{a}{Y} + (n-1)\frac{s}{Y} \sin\Gamma$

This completes the potential solution to the problem.

D. Configurations Used for Evaluation

It was desirable to obtain an evaluation of enough configurations so that effects of channel height, horizontal plate length, and angle of the obstacle could be obtained. Three configurations were selected. The first configuration used an obstacle at 90° to the horizontal and was used as the base from which the other two configurations were selected. The second configuration was also a 90° obstacle of nearly the same height, but with a longer horizontal plate. The third configuration had the same horizontal plate length as the first but the obstacle was 45° to the horizontal. In order to determine the length of the horizontal plate a separation velocity ratio was selected. It was assumed, (subject to verification by means of the viscous solution) that the velocity at the separation point was 91% of the velocity at the leading edge of the plate. The following configurations were determined by analysis:

Configuration	Γ	U/V	S/Y	b/h	c/h	ℓ/h	a/h	Y/h
1	90°	1.15	.97	3.00	.70	3.70	1.00	3.38
2	90°	1.11	1.15	3.33	1.82	5.15	1.00	3.15
3	45°	1.12	1.00	1.81	1.03	2.84	.56	2.53

Configuration number 2 and configuration number 3 had obstacle heights which were a little greater than configuration number 1. However, definite trends are clearly visible as a result of the major changes. The configurations are pictured to scale in Figure 1. The separation points are indicated by S and the attachment points by a.

S - SEPARATION POINT
a - ATTACHMENT PT.

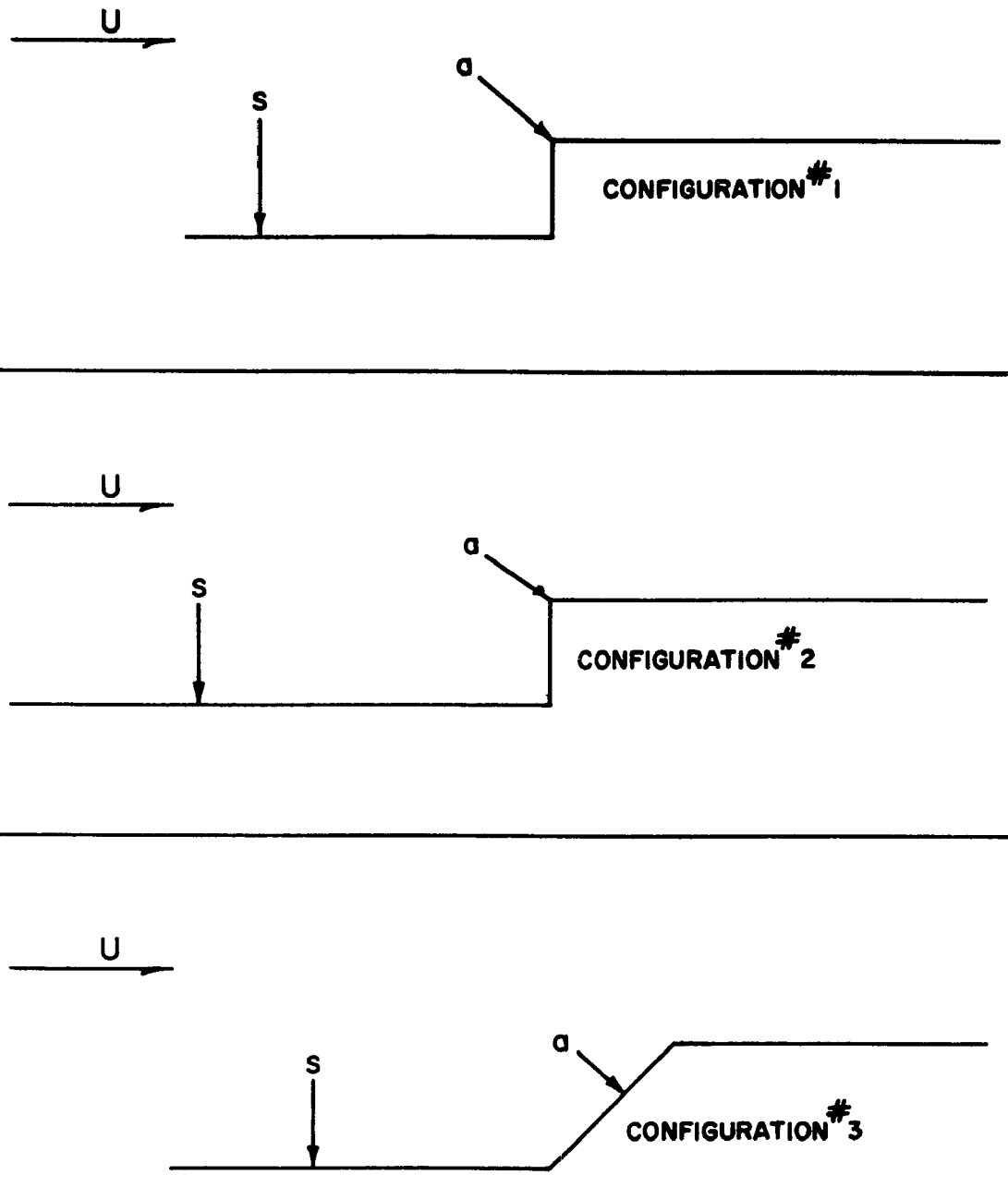

Figure 1. Scale Drawing of the Channel Configurations, Showing Analytical Separation Points.

CHAPTER III

VISCOUS SOLUTION

A. Görtler's Series Solution

Görtler[25] presents a general method for solving the steady laminar boundary layer equations. By introducing the dimensionless variables

$$\xi = \frac{1}{\nu}\int_0^x U(x)\,dx \tag{55}$$

and

$$\eta = \frac{U(x)\,y}{\left\{2\nu\int_0^x U(x)\,dx\right\}^{1/2}} \tag{56}$$

he is able to transform the boundary layer equations into

$$F_{\eta\eta\eta} + FF_{\eta\eta} + \beta(\xi)\left\{1 - F_\eta^2\right\} = 2\xi\left\{F_\eta F_{\xi\eta} - F_\xi F_{\eta\eta}\right\} \tag{57}$$

where

$$F(\xi,\eta) = \frac{\psi(x,y)}{\left\{2\nu\int_0^x U(x)\,dx\right\}^{1/2}} \tag{58}$$

$F(\xi, \eta)$ has the properties that

$$F(\xi,0) = F_\eta(\xi,0) = 0$$

and

$$\lim_{\eta\to\infty} F_\eta(\xi,\eta) = 1$$

Now $\beta(\xi)$ of Equation (57) is given as

$$\beta(\xi) = \frac{2U(x)\int_0^x U(x)\,dx}{U^2(x)} \tag{59}$$

$\beta(\xi)$ is called the "principal function" of the boundary layer equations and the form that $\beta(\xi)$ takes determines the different solutions of the boundary layer equations. As can be seen by (59), not only is $\beta(\xi)$ a function of the local value of the outer velocity and the outer velocity gradient, but it is also a function of the history of the flow upstream from this point.

The outer velocity, which is a result of the potential solution, is written in the form of a power series

$$U(x) = \sum_{k=0}^{\infty} u_k x^k \tag{60}$$

For the case of the incoming flow meeting a cuspidal point, as for flow over a flat plate with a sharp leading edge, (60) takes on the form

$$U(x) = u_0 + u_1 x + u_2 x^2 + u_3 x^3 \cdots \tag{61}$$

with $u_0 \neq 0$, where x is now being measured from the cuspidal point.

As can be seen the main classes of flow can be treated with arbitrary pressure distributions. For this study (61) was the form used for the outer velocity distribution. Equation (61) is then substituted into Equation (55) so that

$$f(x) = \frac{1}{\nu}\sum_{k=0}^{\infty} \frac{u_k x^{k+1}}{k+1} \tag{62}$$

Using the theorem on reversion of power series, x can be expressed as a function of ξ.

$$x(\xi) = c_1\xi + c_2\xi^2 + c_3\xi^3 \cdots \tag{63}$$

Substituting (61) into (59) gives $\beta(\xi)$ as a function of x and the coefficients u_k. From Equation (63) $\beta(\xi)$ can be expressed as a power series of ξ with coefficients β_k:

$$\beta(\xi) = \beta_1\xi + \beta_2\xi^2 + \beta_3\xi^3 \cdots \tag{64}$$

The calculation of $\beta(\xi)$ is now a matter of calculating the coefficients β_k. This can, at least in theory, be easily done.

Putting the power series (64) into the differential Equation (57) gives a solution for $F(\xi,\eta)$ which is a power series in ξ, having coefficients which are functions of η. The coefficients are systems of ordinary differential equations. The first equation is the Falkner and Skan differential equation. All the rest are linear differential equations.

Görtler now reduces the coefficient functions to linear combinations of functions which do not depend on $\beta_1, \beta_2, \ldots, \beta_k$. However, as seems reasonable, he is not able to eliminate the dependence upon β_o. Therefore, β_o is a sort of classifying parameter and for any given β_o universal functions can be obtained and tabulated. The reduction is obtained very neatly and a system of linear differential equations results. These are solved and the results are tabulated in Reference 26.

As previously mentioned it is now desirous to check the assumed velocity reduction. It is proposed to use Görtler's series solution of the boundary layer equations. In applying this new series solution it is first necessary to solve the potential solution from the leading edge of the horizontal plate back to the separation point at B. Equation (39) is this solution in an integral form. Since a closed form of Equation (39) could not be found, a numerical solution was obtained and plotted. This solution was approximated by means of a polynomial. The polynomial was then used in Görtler's series to obtain the wall shear stress and velocity profiles. The discussion of these particulars will follow after introducing Witting's finite difference method.

Görtler[26] carries out the tabulation of the universal functions so that six terms of the series may be evaluated. Therefore, as long as the convergence of the series is sufficiently rapid, six terms is a good approximation to the solution. However, the closer the flow is to the separation point the poorer the approximation. By graphing the partial sums of the wall shear stress, it is possible to determine where this approximation becomes poor. Of course, the necessary degree of accuracy is important here also.

When the accuracy of Görtler's series becomes poor then Witting's finite difference solution must be used.

B. Witting's Finite Difference Solution

In Reference 27 Görtler presents a method of solving the boundary layer equations by means of a finite difference scheme. Witting[28] has improved upon this by a careful consideration of the flow in the vicinity of the wall.

A latticework is set up in which the coordinate points x and y are defined by

$$x_i = x_0 + ih, \quad (i = 0, \pm 1, \pm 2, \cdots, h > 0)$$

$$y_k = \quad k\ell, \quad (k = 0, 1, 2 \cdots, \ell > 0)$$

The velocity u is then given as

$$u_{i,k} = u(x_i, y_k)$$

In finite difference form:

$$\left.\begin{aligned} \frac{\partial u}{\partial x}(x_i, y_k) &= \frac{\Delta_{i,k}}{2h} \quad \text{with} \quad \Delta_{i,k} = u_{i+1,k} - u_{i-1,k} \\ \frac{\partial u}{\partial y}(x_i, y_k) &= \frac{\nabla_{i,k}}{2\ell} \ (k \geq 1) \quad \text{with} \quad \nabla_{i,k} = u_{i,k+1} - u_{i,k-1} \\ \frac{\partial^2 u}{\partial y^2}(x_i, y_k) &= \frac{\nabla^2_{i,k}}{4\ell^2} \ (k \geq 2) \quad \text{with} \quad \nabla^2_{i,k} = \nabla_{i,k+1} - \nabla_{i,k-1} \end{aligned}\right\} \quad (65)$$

Then

$$\nabla_{i,0} = 2\ell \frac{\partial u}{\partial y}(x_i, 0)$$

and

$$\nabla^2_{i,0} = 4\ell^2 \frac{\partial^2 u}{\partial y^2}(x_i, 0)$$

where

$$\frac{\partial^2 u}{\partial y^2}(x_i, 0) = -U \left.\frac{dU}{dx}\right|_{x = x_i} \quad (66)$$

Using the continuity equation gives

$$v_{i,k} = -\int_0^{y_k} \frac{\partial u}{\partial x}(x_i, y)\, dy$$

and with the help of the Trazezoidal rule this can be written

$$v_{i,k} = -\left(\sum_{r=1}^{k-1} \frac{\Delta_{i,r}}{2h} + \frac{1}{2}\,\frac{\Delta_{i,k}}{2h}\right)\ell \tag{67}$$

If $u_{i,k} - \frac{1}{4}\nabla_{i,k} \neq 0$, then substituting the above system into the boundary layer equation gives

$$\Delta_{i,k} = \frac{4h(UU')_i + \frac{h}{\ell^2}\nabla_{i,k}^2 + \nabla_{i,k}\sum_{r=1}^{k-1}\Delta_{i,r}}{2\left(u_{i,k} - \frac{1}{4}\nabla_{i,k}\right)} \tag{68}$$

In order to determine the quantities $\nabla_{i,o}$ and $\nabla_{i,1}^2$, the velocity distribution in the vicinity of the wall is approximated by a polynomial

$$\hat{u}_i(y) = b_o y + \frac{\nabla_{i,o}^2}{8\ell^2} y^2 + \sum_{s=4}^{k} \frac{b_s}{s!} y^s \tag{69}$$

The coefficients $b_o, b_4, \ldots, b_k$ are determined from known profiles or beginning profiles. Also for the known profiles as a result of (69) the values

$$\nabla_{i,o} = 2\ell \left.\frac{\partial \hat{u}_i}{\partial y}\right|_{y=o} \tag{70}$$

and

$$\nabla_{i,1}^2 = 4\ell^2 \left.\frac{\partial^2 \hat{u}_i}{\partial y^2}\right|_{y=\ell} \tag{71}$$

may be found. Further, if it is assumed that the relation between $\hat{u}_i(y)$ and $u_{i,r}$ is linear then from (69), (70), and (71)

$$\nabla_{i,0} = A_0 \nabla_{i,0}^2 + \sum_{r=1}^{5} A_r u_{i,r} \tag{72}$$

$$\nabla_{i,1}^2 = B_0 \nabla_{i,0}^2 + \sum_{r=1}^{5} B_r u_{i,r} \tag{73}$$

where k has been picked as 5. From known velocity profiles the coefficients A_r and B_r can be determined.

Witting points out that irregularities in the velocity profile can become exaggerated because of the denominator of Equation (68). These irregularities are pronounced along the line $y = \ell$ and become greater near the separation point. To overcome this he introduces another method of evaluation of the velocity profile for points near the surface. Witting approximates the velocity $u(x_i,y)$ by the polynomial

$$\hat{u}_i(y) = \frac{\nabla_{i,0}}{2\ell} y + \frac{\nabla_{i,0}^2}{8\ell^2} y^2 \tag{74}$$

Since the continuity equation gives

$$v_{i,k} = -\int_0^{y_k} \frac{\partial u}{\partial x} \, dy$$

and

$$\frac{\partial u}{\partial x}(x_i,y) = \frac{\Delta_{i,k}}{2h} = \frac{u_{i+1,k} - u_{i-1,k}}{2h}$$

then

$$v_{i,k} = -\frac{1}{2h} \int_0^{y_k} (u_{i+1,k} - u_{i-1,k}) \, dy \tag{75}$$

Substituting (74) into (75) gives

$$v_{i,k} = -\left(\nabla_{i+1,0} - L_{i,k}\right)\frac{k^2 \ell}{8h} \tag{76}$$

where

$$L_{i,k} = \nabla_{i-1,0} - k/6\left(\nabla^2_{i+1,0} - \nabla^2_{i-1,0}\right) \tag{77}$$

This value of $v_{i,k}$ is now used for $k = 1$ and $k = 2$. Therefore, when substituted into the boundary layer equations, it gives

$$\Delta_{i,k} = \frac{1}{2u_{i,k}}\left[\left(\nabla_{i+1,0} - L_{i,k}\right)\nabla_{i,k}\frac{k^2}{4} + 4h\left(\overline{uu'}\right)_i + \frac{h}{\ell^2}\nabla^2_{i,k}\right] \tag{78}$$

For $k \geq 3$ he uses Equation (68). Therefore, to overcome these irregularities Witting has come up with two finite difference equations. One equation is used for $k = 1$ and $k = 2$ and the other equation is used for $k \geq 3$. However, in so doing he has introduced an additional difficulty. The calculation of $\Delta_{i,k}$ for $k = 3$ depends upon the calculation of $\Delta_{i,k}$ for $k = 1$ and $k = 2$. These, as can be seen from (78), depend upon $\nabla_{i+1,0}$ and $\nabla^2_{i+1,0}$. But according to (72) $\nabla_{i+1,0}$ cannot be calculated until the velocity points $u_{i+1,k}$ are calculated. However, Witting points out that there are six linear relations between the six quantities $\nabla_{i+1,0}, \Delta_{i,1}, \ldots, \Delta_{i,5}$. These are Equations (78) and (68) and

$$\nabla_{i+1,0} = A_0 \nabla^2_{i+1,0} + \sum_{r=1}^{5} A_r u_{i+1,r} \tag{79}$$

Using these he sets up an iteration scheme, whereby $\nabla_{i+1,0}$ is assumed

so that the process can get underway. Then, as he shows, this assumption is checked by means of

$$\nabla_{i+1,0} = K_i + \sum_{r=1}^{5} A_r \Delta_{i,r} \tag{80}$$

which is a direct result of substituting (78) and (68) into (79) and using $\Delta_{i,k} = u_{i+1,k} - u_{i-1,k}$.

For the application of the finite difference method, Witting sets up a convenient scheme and outlines a useful schedule.

First, he suggests the calculation of

$$N_{i,k} = \begin{cases} 2u_{i,k} & (k=1,2) \\ 2\left(u_{i,k} - \tfrac{1}{4}\nabla_{i,k}\right) & (k \geq 3) \end{cases} \tag{81}$$

$$Z_{i,k} = 4h(UU')_i + \frac{h}{l^2}\nabla_{i,k}^2 = \frac{h}{l^2}\left(\nabla_{i,k}^2 - \nabla_{i,0}^2\right) \quad (k \geq 1) \tag{82}$$

along with the quantities $\nabla_{i,k}$, $\nabla_{i,k}^2$, and $\frac{1}{4}\nabla_{i,k}$.

Using (81) and (82) Equations (78) and (68) become

$$\Delta_{i,1} = \frac{1}{N_{i,1}}\left[\left(\nabla_{i+1,0} - L_{i,1}\right)\frac{\nabla_{i,1}}{4} + Z_{i,1}\right] \tag{83}$$

$$\Delta_{i,2} = \frac{1}{N_{i,2}}\left[\left(\nabla_{i+1,0} - L_{i,2}\right)\nabla_{i,2} + Z_{i,2}\right] \tag{84}$$

$$\Delta_{i,k} = \frac{1}{N_{i,k}}\left[S_{i,k}\nabla_{i,k} + Z_{i,k}\right] \tag{85}$$

where

$$S_{i,k} = \sum_{r=1}^{k-1} \Delta_{i,r} \tag{86}$$

Next he suggests the calculation of the quantities $\nabla^2_{i,0}$, $\nabla_{i,0}$, $\nabla^2_{i,1}$, K_i, $L_{i,1}$, and $L_{i,2}$. After these one is in a position to start the iteration to determine $\nabla_{i+1,0}$. Assume a value of $\nabla_{i+1,0}$. After a few velocity profile calculations, a good estimate of $\nabla_{i+1,0}$ can be made. For the assumed $\nabla_{i+1,0}$ calculate $\nabla_{i,r}(r = 1,2,3,4,5)$ according to (83), (84), (85) and (86). Then check this assumption by means of (80). After $\nabla_{i+1,0}$ is obtained, then one can proceed to finish out the velocity profile by means of (85) and (86).

The size of the latticework depends upon the desired accuracy and the proximity to the separation point. Witting suggests that ℓ should be chosen so that there are 15 points in each velocity profile. Also after a few calculations of the velocity profile are made, it is necessary to perform a smoothing process; since for any given value of k irregularities propagate in the direction of flow. This smoothing can be done graphically or algebraically. It is also desirable to reduce the size of the steps, h, the closer one gets to the separation point. This increases the accuracy.

To start the process it is necessary to have two velocity profiles, $u_{-1,k}$ and $u_{0,k}$. These two profiles must be h distance apart and must be calculated by some scheme other than the finite difference process. This is where Görtler's series solution and Witting's finite difference method join together. Görtler's series solution is used to

calculate $u_{-1,k}$ and $u_{0,k}$ at the point where it is felt that the accuracy of Görtler's series is becoming questionable.

C. Application of Görtler's Series and Witting's Finite Difference Method

To check the validity of the assumed velocity reduction in Chapter II, Görtler's series and Witting's finite difference method were used to solve the boundary layer equations and obtain the wall shear stress.

Returning to the potential solution, Equation (39) gave

$$X/Y = \frac{U}{\pi V}\int_0^{\beta'} e^{-\beta'} d\{\ln[-N\tan^2(P\beta', k')+1]\}$$

This equation was solved graphically to obtain values of $-x/Y$ versus q/V. $-x/Y$ can be transformed to $-x/h$ by multiplying by Y/h. Plotting q/V versus $-x/h$ graphically represents the potential velocity distribution along the plate from the separation point forward into the oncoming flow. The velocity q/V will be unity at the separation point and will increase with $-x/h$. A value of q/V is picked for the leading edge. This gives $-x/h$ up to the leading edge, so that c/h equals $-x/h$ at the leading edge.

Now if each value of q/V is divided by the selected value of q/V for the leading edge, a dimensionless velocity $\bar{U}$ results, which is unity at the leading edge and decreases up to the separation point. The value of $\bar{U}$ at the separation point is defined as the separation velocity. Then for each value of $\bar{U}$, an $\bar{x}$ is calculated by transforming $-x/h$, so that $\bar{x} = -x/h + (x/h)_{l.e.}$ where $(x/h)_{l.e.}$ is the value of (x/h) at the leading edge. The final results are that at $\bar{x} = 0$,

$\bar{U}(\bar{x}) = 1.0$, and as $\bar{x}$ increases in the direction of flow $\bar{U}(\bar{x})$ decreases until separation is reached. The selected value of $\bar{U}(\bar{x})$ at separation was .91. This is the value assumed by Lighthill in his analysis. It is used here as a first estimate.

Figure 2 shows the graph of $\bar{U}(\bar{x})$ versus $(\bar{x})$ for configuration number 1. An important point should be made here about this solution. Near the separation point the velocity dips noticeably, so that at separation the gradient of $\bar{U}(\bar{x})$ is infinite. Referring to Euler's equation, this means that the force per unit mass must be infinite at this point. Physically this is impossible.

In order to use this velocity distribution in Görtler's series it must be approximated by a polynomial. A third degree polynomial was used. It was felt that this would give sufficient accuracy and its calculation could be easily carried out by hand. Also, since the real outer velocity distribution could not approach that of the potential solution near the separation point, the polynomial closely approximated the potential solution everywhere but at separation. The circles of Figure 2 indicate the points used for calculation of the polynomial and the dashed line is the polynomial approximation. For configuration number 1,

$$\bar{U}(\bar{x}) = 1.0000 - .05464\bar{x} + .03185\bar{x}^2 - .14918\bar{x}^3 \qquad (87)$$

Görtler shows (Reference 25, p. 15) that dimensionless quantities can be used in the new series, where as defined above $\bar{x} = -x/h + (x/h)_{se}$

$$\bar{U}(\bar{x}) = \frac{U(x)}{U_o} \qquad (88)$$

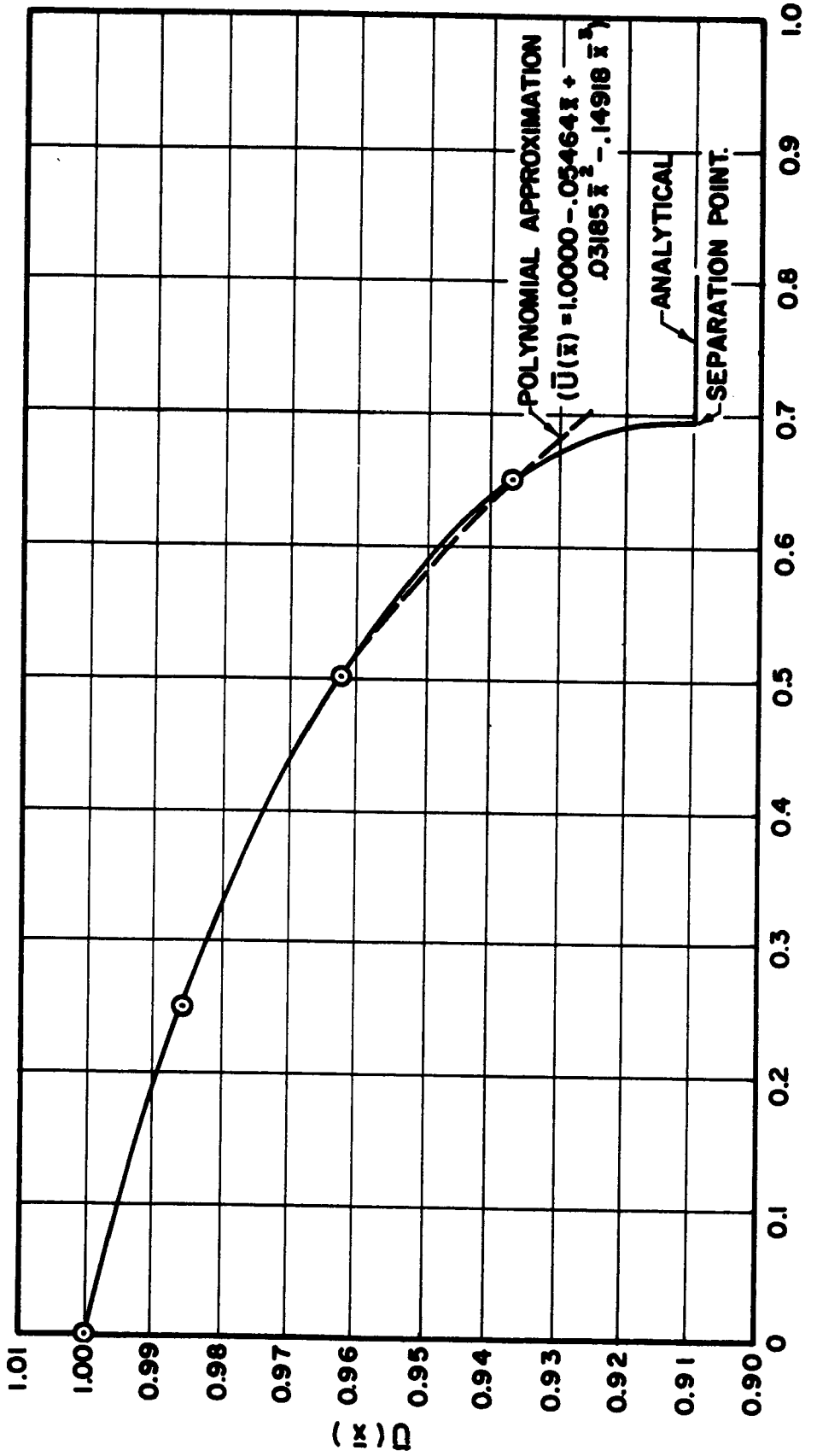

Figure 2. $\bar{U}(\bar{x})$ vs. $\bar{x}$ for Configuration Number 1.

U_o is the velocity at $x = 0$. Then

$$\bar{u}_k = \frac{u_k h^k}{U_o}$$
$$\bar{\xi} = \xi / R_e \tag{89}$$

where

$$R_e = \frac{U_o h}{\nu} \tag{90}$$

and

$$\bar{\beta}_k = \beta_k R_e^k \tag{91}$$

He goes on to show that the series can be used as is, if β_k is replaced by $\bar{\beta}_k$ and along with this a_k is replaced by $\bar{u}_k$. a_j is an abbreviation for $\nu^j u_j / U_o^{j+1}$, which is a result used in finding the coefficients βk. Referring to Equation (87)

$$\begin{aligned} \bar{u}_0 &= 1.0000 \\ \bar{u}_1 &= -.05464 \\ \bar{u}_2 &= +.03185 \\ \bar{u}_3 &= -.14918 \end{aligned} \tag{92}$$

To determine separation the wall shearing stress is needed. Görtler shows that

$$\bar{F}_k = F_k R_e^k$$

and accordingly from (58)

$$\frac{\partial \bar{u}}{\partial \bar{y}}\Big|_{\bar{y}=0} = \bar{U}(\bar{x})\, \bar{q}(\bar{x}) \sum_k \bar{F}_k''(0)\, \bar{\xi}^k \tag{93}$$

where

$$\bar{g}(\bar{x}) = \frac{\bar{U}(\bar{x})}{\sqrt{2\,\bar{\xi}(\bar{x})}} \tag{94}$$

Perform the following transformation of variables,

$$\bar{\xi} = \int_0^{\bar{x}} \bar{U}(\bar{x})\, d\bar{x} \tag{95}$$

$$\eta = \bar{\eta} = \bar{g}(\bar{x})\,\bar{y} \tag{96}$$

where

$$\bar{y} = \frac{y R_e^{1/2}}{h} \tag{97}$$

Next calculate the coefficients $\bar{\beta}_k$, which are given on p. 14 of Reference 25. For configuration number one:

$$\bar{\beta}_0 = 0$$
$$\bar{\beta}_1 = -.109276$$
$$\bar{\beta}_2 = .115468$$
$$\bar{\beta}_3 = -.872020$$
$$\bar{\beta}_4 = -.185187$$
$$\bar{\beta}_5 = .088508$$

$\bar{F}_k''(0)$ can be calculated according to p. 41 and 42 of Reference 25 and are:

$$\bar{F}_0''(0) = 0.469600$$
$$\bar{F}_1''(0) = -0.112812$$

$$\bar{F}_2''(0) = 0.096324$$
$$\bar{F}_3''(0) = -0.710183$$
$$\bar{F}_4''(0) = -0.246474$$
$$\bar{F}_5''(0) = +0.108221$$

The wall shearing stress was calculated for $\bar{x}$, starting at $\bar{x} = .10$, in steps of .10 up to $\bar{x} = .70$. Partial sums of (93) were made and these results are plotted on Figure 3. Referring to these partial sums of the wall shear stress, the rapidity of convergence can be gauged. It was felt that for good accuracy, Görtler's series could not be used beyond $\bar{x} = .40$, because of the results in Figure 3.

To pick up at this point with Witting's finite difference method it was necessary to calculate two velocity profiles; one for $u_{-1,k}$ and the other for $u_{0,k}$. h was selected as .04 so that $u_{-1,k}$ was at $\bar{x} = .36$ and $u_{0,k}$ was at $\bar{x} = .40$.

$$\bar{u}(\bar{x},\bar{y}) = \bar{U}(\bar{x}) \sum_k \bar{F}_k'(\eta)\bar{\xi}^k \tag{98}$$

The tables of Reference 26 were used to determine $\bar{F}_k'(\eta)$.

Witting suggests the use of the following for $\nabla_{i,0}$ and $\nabla^2_{i,1}$:

$$\nabla_{i,0} = -0.47347\nabla^2_{i,0} + 1.79091\,u_{i,3} - 1.13331\,u_{i,4} + .23210\,u_{i,5} \tag{99}$$

and

$$\nabla^2_{i,1} = 0.68972\,\nabla^2_{i,0} - 1.43631\,u_{i,3} + 1.53392\,u_{i,4} - .36535\,u_{i,5} \tag{100}$$

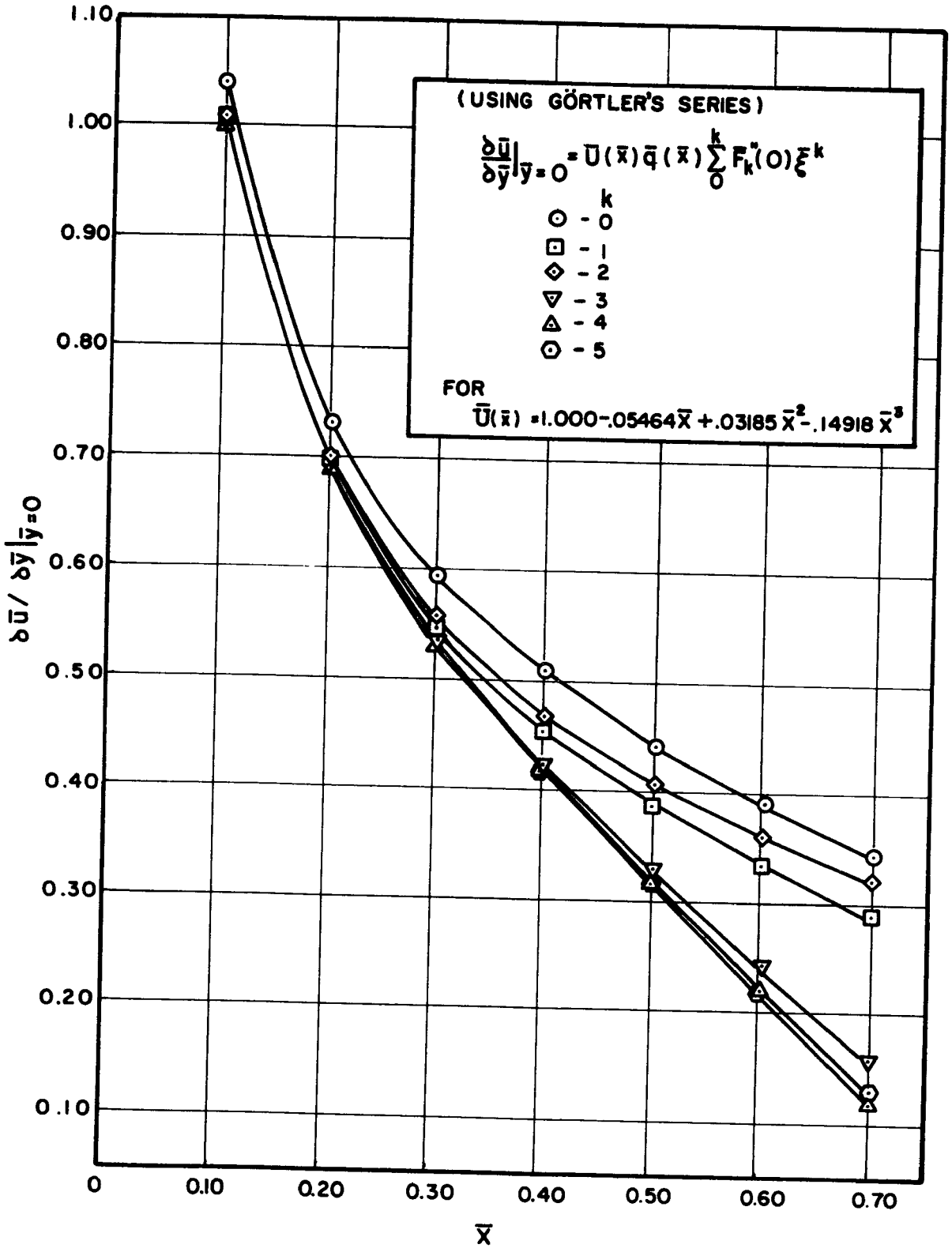

Figure 3. $\frac{\partial \bar{u}}{\partial \bar{y}}\Big|_{\bar{y}=0}$ vs. $\bar{x}$ for Configuration Number 1.

In order to check the accuracy of (99) and (100)

$$\hat{u}_i(y) = by + \frac{\nabla_{i0}^2}{8\ell^2} y^2 + \frac{b_4}{4!} y^4 + \frac{b_5}{5!} y^5 \qquad (69)$$

was calculated for the velocity profile at $\bar{x} = .40$. Then by using the calculated velocity points in (99) and (100), $\nabla_{i,0}$ and $\nabla^2_{i,1}$ were compared with those obtained by means of (69). It was found that (99) was within .3% of (69) for the value of $\nabla_{i,0}$ and within 2.5% for the value of $\nabla^2_{i,1}$. It was felt that this accuracy was very good so that the finite difference method was carried out using (99) and (100).

The distance ℓ was picked equal to .3652 and 18 points were picked for the $\bar{y}$ direction. In order to determine the values of $u_{-1,k}$ for $\bar{y} = k\ell$ ($\ell = .3652$ and $k = 0,1,2,\ldots,18$) it was necessary to graph $u_{-1,k}$ as calculated by Görtler's series. Starting with $\bar{x} = .40$ for $u_{0,k}$, h was equal to .04 for 4 steps. h was reduced to .02 for the next 6 steps and then equal to .01 for the last two steps.

A graph of $\left.\frac{\partial \bar{u}}{\partial \bar{y}}\right|_{\bar{y}=0}$ versus $\bar{x}$ is shown in Figure 4. It indicates that separation occurs at $\bar{x} = .707$. This agrees very well with the $\bar{x}$ at separation which results from selecting $\bar{U}(\bar{x}) = .91$ at separation, see Figure 2. This was therefore taken to be the analytical verification of the selection of .91 for the velocity reduction to separation.

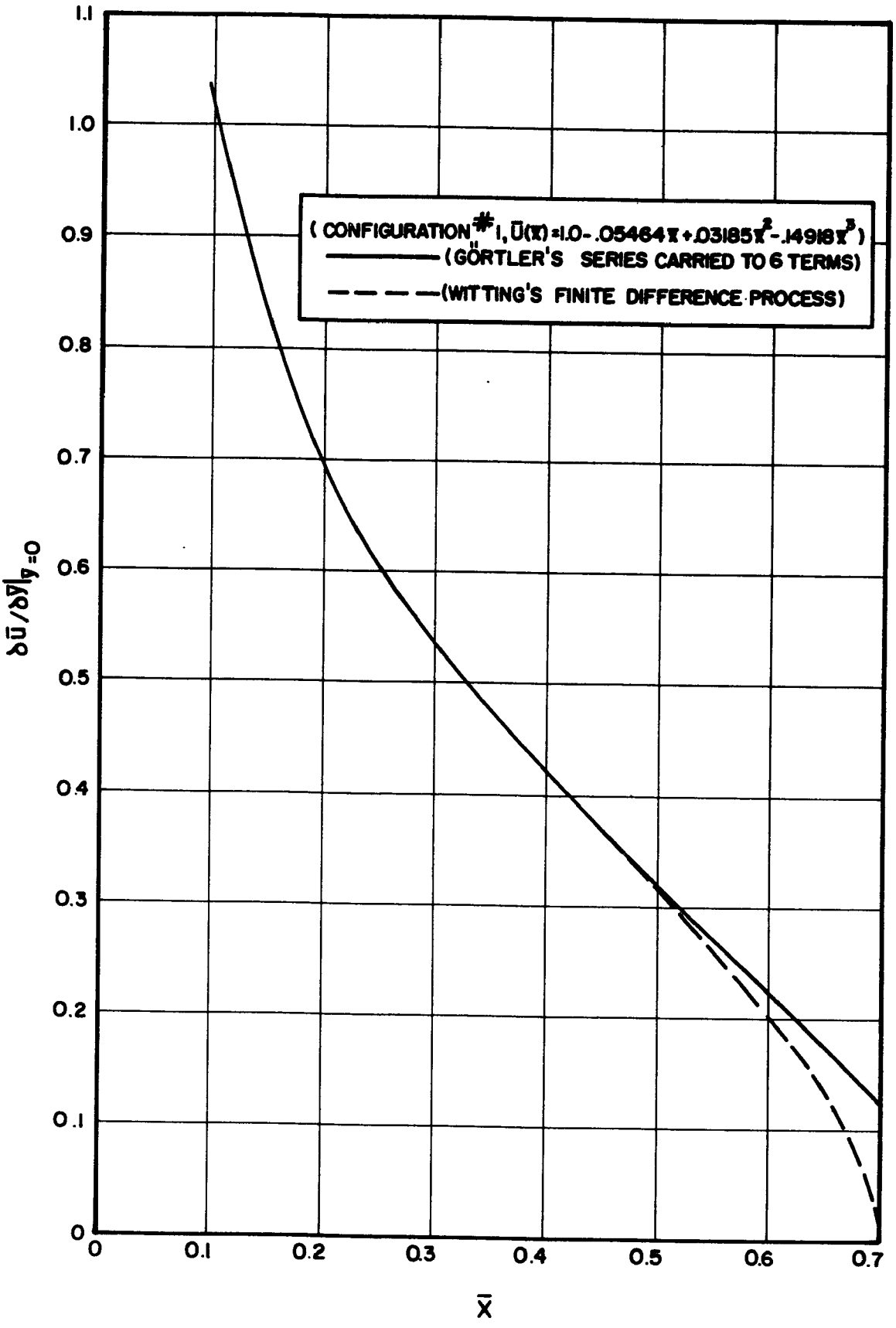

Figure 4. Plot of $\frac{\partial \bar{u}}{\partial \bar{y}}\Big|_{\bar{y}=0}$ vs $\bar{x}$ for Analytical Velocity $\bar{U}(\bar{x})$ for Configuration Number 1.

CHAPTER IV

EXPERIMENTAL INVESTIGATION

The experimental program was carried out to evaluate the analysis. Three configurations were used; the same configurations that are listed on p. 32 . The program consisted of static pressure measurements along with flow visualization techniques. The testing medium was air which was supplied by a compressor-settling plenum arrangement. Testing was done in the Mechanical Engineering Department's Fluid Flow Laboratory in the Fluid Engineering Building.

A. Basic Test Equipment

The basic equipment consisted of a Joy Model B air compressor with a 100 HP drive, producing 550 cfm of free air. The compressed air discharged into a receiver storage tank before being channeled to various parts of the building. The test rig which was supplied by a 2 inch pipe is shown in Figure 5. A Cuno Model No. 6F IG air filter was used to remove oil, water, rust or any large contamination from the air stream. Following this a Fischer-Governor control valve was mounted. Because of difficulty in controlling the flow rate with this valve, it was left fully open during all running. The flow rate was controlled by means of bleed off at the back of the rig. During operation, after steady flow had been achieved, the compressor ran at a constant load, so that air flow fluctuations were minimized. Also, all running was done at hours that insured minimum use of the air supply by anyone else.

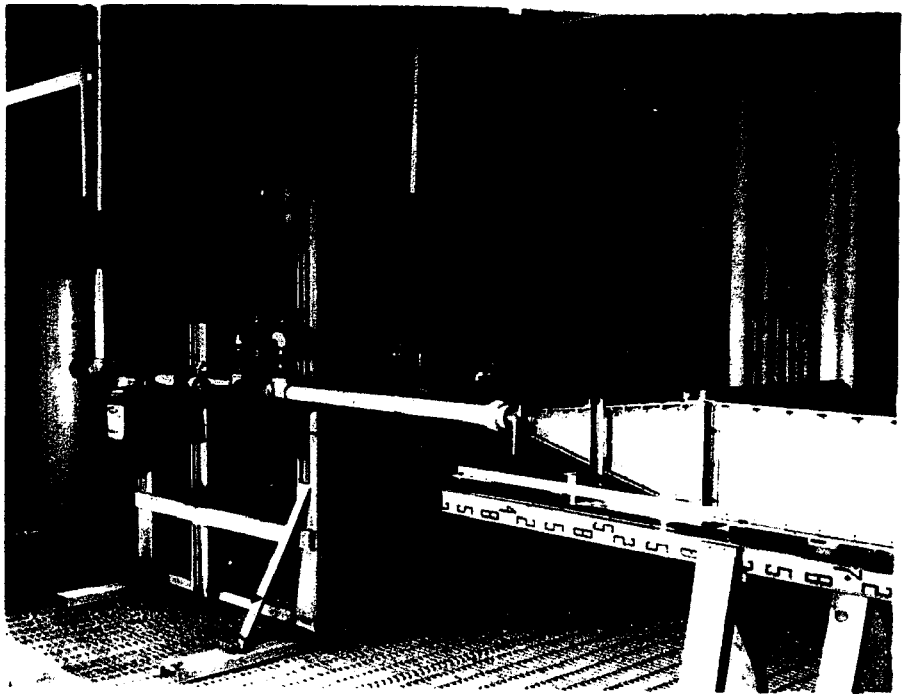

Figure a. View of Filter Assembly and Control Valve at Plenum Chamber Entrance.

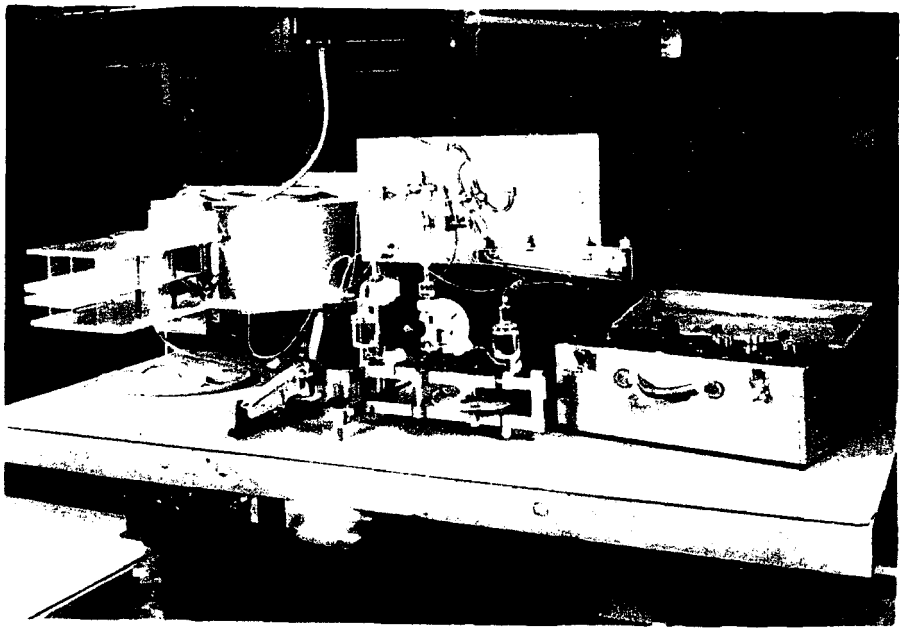

Figure b. View of Test Channel and Instrumentation.

The settling plenum was located downstream of the Fischer valve. This plenum was obtained from the Aeronautical and Astronautical Engineering Department and was fitted with a contraction section at the discharge to insure a smooth acceleration of the air flow before it engaged the test section.

The settling plenum was made up of an aluminum frame and covering. It had a wooden liner which supported eleven screens. After the air entered from the 2 inch pipe, it was decelerated by a diverging section. This section was 32 inches long and contained four of the eleven screens; each screen had 150 wires to the inch. The main chamber had a cross sectional flow area of 23" x 10" and was 78" long. The seven equally spaced screens in it had 50 wires to the inch.

The contraction section had a 7.66 to 1 contraction ratio. It was 18 inches long and the outlet was 5" x 6". The test section was located at the discharge of the contraction section. It was rigidly mounted to the end of the contraction section. The air flow which issued from the contraction section flowed through the test section and then into the open room.

B. Test Channels

The discharge from the contraction section was 6 inches high and 5 inches wide. The test sections were located so that the leading edge of the horizontal plate was 3 inches from this discharge plane. To insure a uniform flow and an even boundary layer build up the horizontal plate was located midway in the channel height. This meant that Y of the potential solution was 3 inches. The horizontal plate was made of

.053 inch stainless steel. The stainless steel was used to insure a smooth hard surface which would resist being scratched. The bottom side of the leading edge was sharply tapered so that the top of the horizontal plate was used for the test section. The sharp leading edge reduced the stagnation effect and permitted a smooth build up of the boundary layer along the upper surface. The horizontal plate was maintained parallel to the flow by the side walls of the test section. These walls were made of 1/4 inch plexiglass in which grooves were machined to hold the horizontal plate. The grooves were machined perpendicular to the forward face of the side walls, so that a zero angle of attack of the air over the horizontal plate resulted when the test section was bolted to the plenum discharge.

The top and bottom of the test section were made of 1/2 inch plexiglass which extended beyond the sidewalls. Through bolts were used on the outside of the sidewalls to clamp the test section together into a rigid body. The obstacles were made of plexiglass, which were cut to fit the straight channel. The plexiglass obstacles were shimmed to the correct height and bolted together by a tie bolt. In the top of the test section a removable section was machined to enable easy access to the test plate after the section was installed.

All three configurations could be made from the same test section pieces. The obstacle height could be changed by shimming and its location from the leading edge was altered by cutting a new location hole in the horizontal plate. The 45 degree obstacle was machined and therefore required special pieces.

Although the test section itself was only 5 inches wide by 3 inches high, a wide area of two dimensional flow was obtained. This was verified by surface patterns of china clay and smoke studies.

All instrumentation was brought out through the test section walls by cutting holes. These holes were sealed adequately to insure minimum leakage. A typical build up of one test section configuration is shown in Figure 6.

C. Test Instrumentation

In the investigation a number of experimental approaches were used in an effort to produce checks upon one another. Flow visualization was obtained by use of smoke traces. Attempts at surface visualization were made by use of china clay techniques and talcum powder and oil techniques. Static pressures were also taken along the plate.

1. Talcum Powder Generator

An interesting addition to the technique of surface visualization was made by Chang and Dunham.(29) They showed how separation could be found by spraying a mist of fine talcum powder over a surface which is wetted with a thin film of oil. They used a strut to demonstrate the technique. The mist of talcum powder was introduced into the wake of the strut and supposedly the reversed flow carried the powder forward, depositing it on the surface of the oiled strut as far forward as the separation point. Ahead of separation the surface was swept clean. This approach was used here. A section of 1 inch pipe 4 inches long was used to hold the talcum powder. The pipe was capped on both ends and small brass tubes were inserted and brazed into the iron caps. This produced a container

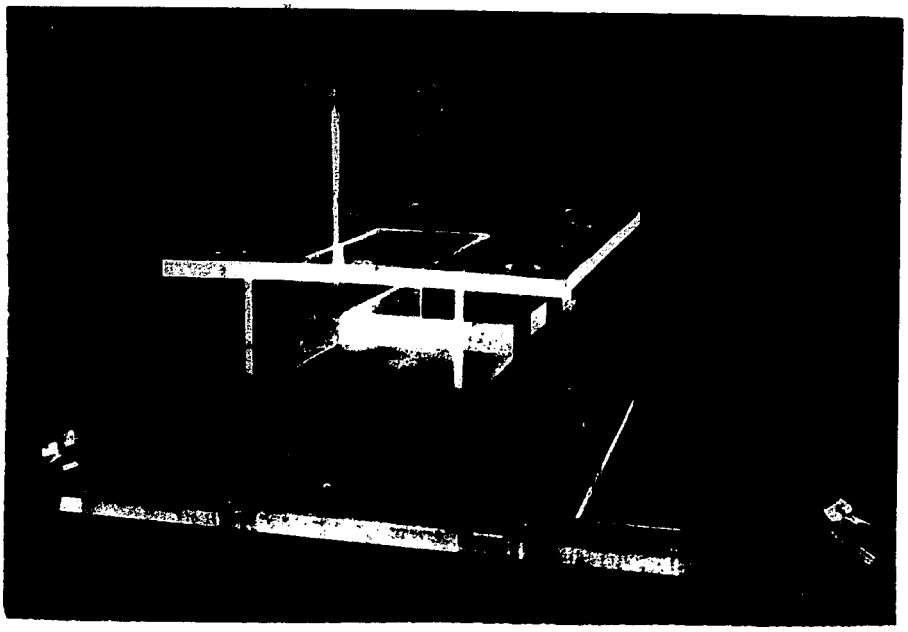

Figure 6. Typical Build Up of Test Section Showing Static Pressure Instrumentation.

which could withstand the shop air pressures necessary to get a good mist of powder. Shop air was introduced at one end in such a way that a vortex was produced in the container. The mixture of air and talcum powder was then removed through a 1/32 inch inside diameter rubber tube to a spray tube. The spray tube was made of 1/16" O.D. brass tubing which was inserted on either side of the test section in the area of the corner, well into the separated zone. The end of the spray tube was bent forward so that the talcum powder would be ejected outward from the side walls and a little forward so as to fill out the separated region. The horizontal plate which was coated with a very thin film of oil was painted black. This gave a very good contrast and a sharp line of demarcation resulted between white and black.

2. Smoke Generator

Smoke traces were used to get an idea of the flow behavior in the separated region. The smoke producing substance in this apparatus was oil soaked cigars. When lighted and operated with the proper air flow rate the smoke was very thick and white. Regulated shop air was led through an iron pipe which contained two cigars. (See Figure 7.) About 1/2 of a 10 c.c. syringe of light machine oil was injected into each cigar. The smoke, which was produced by lighting the cigars, was then bubbled through water which was contained in a 1000 c.c. flask. This flask was surrounded by an ice water bath. It was hoped that the ice water bath would appreciably lower the temperature of the smoke, so that moisture and products of combustion would condense and therefore produce a denser smoke. Regulation of the smoke flow rate was obtained by throttling the inlet air and also bleeding off smoke from the flask.

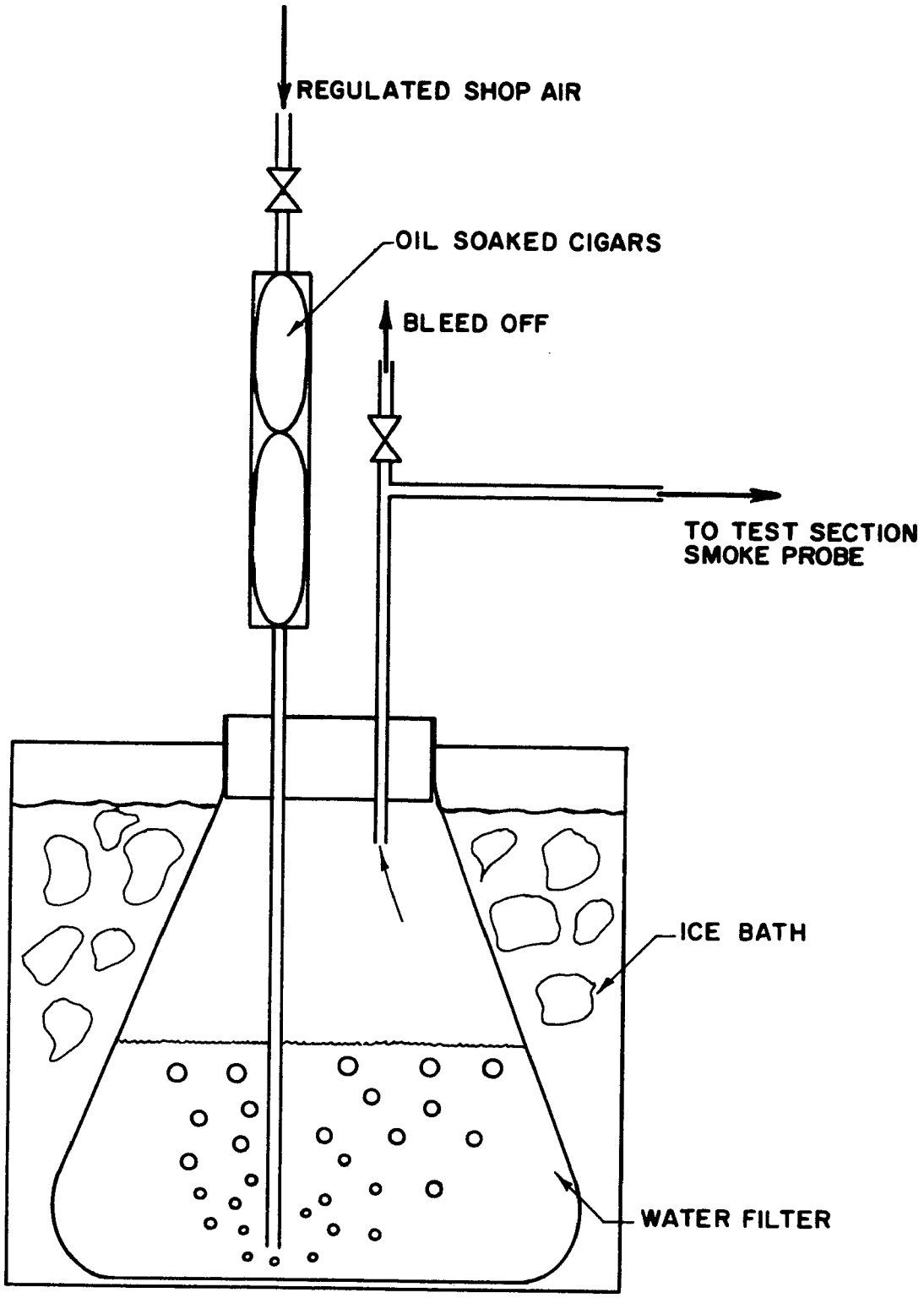

Figure 7. Schematic of Smoke Generator.

From the flask outlet the smoke was led through 1/32" I.D. rubber tubing to the smoke discharge probe. This probe was mounted vertically from the bottom of the test section. The probe was made of 1/16" O.D. by 1/64" wall thickness brass tubing and was curved to about 45° with the horizontal at the very end. The purpose of mounting the probe from the bottom was to allow the smoke to discharge from the probe in a plane which was below the horizontal plate and to eliminate any interference of the probe with the airstream in the upper half of the test section. The probe was also mounted so that it could traverse across the test section. Because of the attitude of the end of the probe the smoke issued in the downstream direction and also upward. A smooth stream of smoke with no interference from the probe was obtained when the smoke velocity was matched with the velocity of the airstream.

3. Static Pressure Instrumentation

Static pressure taps were installed in a .053 inch thick stainless steel plate. Sixteen holes of .024 inch diameter were drilled through the plate. The sixteen holes were arranged as shown in Figure 8. The purpose of this arrangement was to reduce the probable interference of one hole with another and still obtain enough pressure taps in the direction of flow to get an accurate evaluation of the pressure variation over the horizontal plate surface. In order to avoid dimpling the plate when marking the hole location and thereby introduce error into the measurement, an aluminum template was made with the desired hole size and pattern. Then this template was used to guide the drill during the marking of the holes. A high speed drill was used to cut the holes.

Kerosene was used as a cutting fluid to improve the cut. The holes were drilled from the top surface down to avoid burrs on the upper surface, (this being used as the flow surface). Following drilling, the holes were honed by using the drill shank and 440 fine carborundum compound. The carborundum was placed around the drill shank and the drill shank was rotated in the holes to smooth the holes and remove any burrs. Zero error in pressure measurement could not be achieved, as pointed out in Reference 30. Using Reference 30 as a guide, and by maintaining the hole's length/diameter ratio as high as possible the error could be reduced. The hole size was selected in keeping with the minimum hole diameter, that could conveniently be cut, and the thickness of the plate.

Starting with the hole closest to the leading edge which was labeled number one, each hole was numbered consecutively. The rows were 1/4 inches apart and nominally the holes were 3/16 inches apart in the downstream direction.

Hole No.	Distance from leading edge	Row No.
1	.374 inches	2
2	.558 inches	3
3	.741 inches	1
4	.934 inches	2
5	1.112 inches	3
6	1.296 inches	1
7	1.499 inches	2
8	1.714 inches	3
9	1.867 inches	1
10	2.052 inches	2
11	2.250 inches	3
12	2.421 inches	1
13	2.624 inches	2
14	2.812 inches	3
15	2.991 inches	1
16	3.187 inches	2



Figure 8. View of the Static Pressure Hole Locations.

A major problem during this installation was obtaining leads from the holes out to a measuring instrument and still not obstruct the flow path so that major shifts in flow would result. After one unsuccessful attempt, it was decided to use 16 gauge stainless steel hypodermic tubing. The tubing was cut in lengths which reached from the hole out beyond the side walls of the channel. A small flat was ground on the side of the tube near one end. In this flat a .024 inch diameter hole was drilled. This hole was matched to a hole in the plate and the tube was secured in place by Epoxy cement. The Epoxy cement was also used to seal off the open end of the tube which was near the pressure hole. (See Figure 9.) The tubes after being secured lay flat against the surface of the plate and increased the effective thickness of the plate by only .065 inches. Because of disturbances which might be caused at the leading edge, the first hole was drilled at 3/8 inches from the leading edge, but each subsequent hole was drilled at intervals of approximately 3/16 inches. The leading edge was sharply tapered along the bottom surface.

Rubber tubes 1/32" inside diameter were attached to the outside end of each steel tube and led to the pressure recording instrument. Each hole was pressure checked to 6 inches of water gauge, with no leaks indicated. Since this pressure was well beyond the pressure differentials expected this was felt to be sufficient proof of adequate sealing.

4. Pressure Recording

Pressure differentials were recorded by means of a Chattock-Fry tilting manometer. This instrument is a U-tube with a special means of

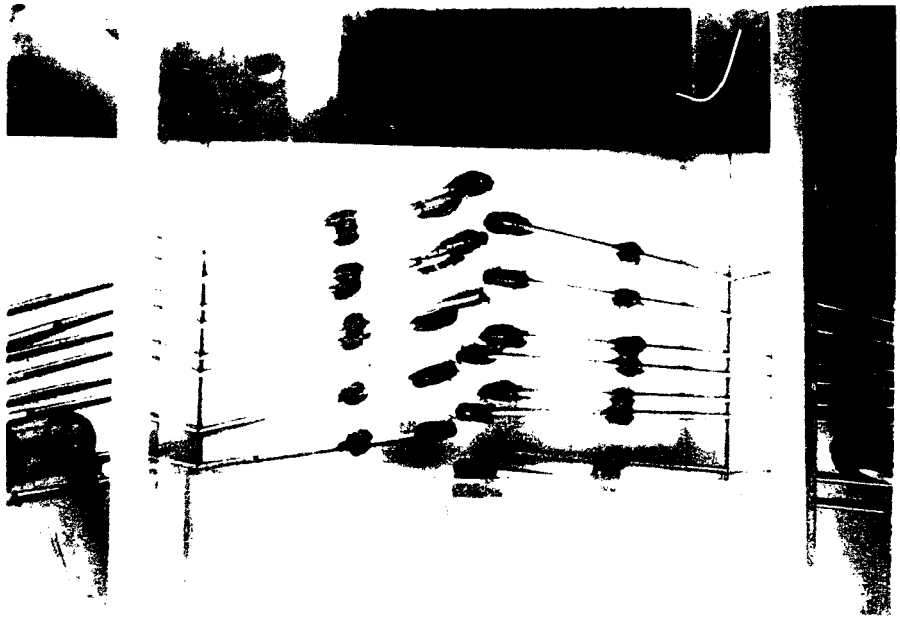

Figure 9a. View of Bottom of Test Section Showing Static Pressure Instrumentation.

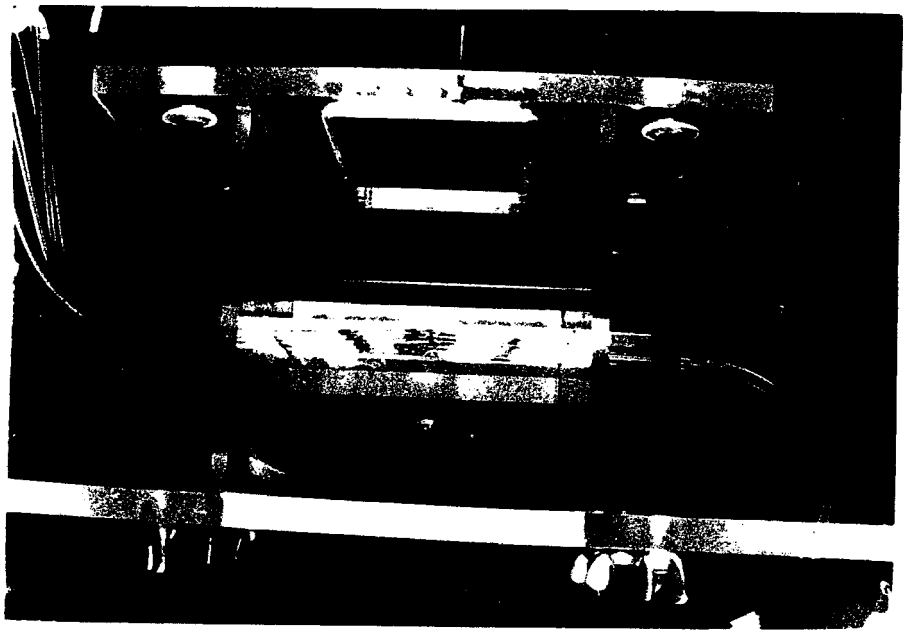

Figure 9b. View of Test Section Showing Static Pressure Instrumentation.

observing any difference in level between two separated water reservoirs. The water reservoirs are at the ends of the U-tube assembly. At the center of one leg of the U-tube is located a central chamber. The center portion of the other leg fits through the center of the bottom of this central chamber in a short vertical tube which is ground off flat at the top. Each leg of the U-tube assembly is fitted with taps which can shut off either or both of the reservoirs from the central portion of the gauge. Distilled and deaerated water is placed in each leg and mineral oil is placed in the central chamber, so that two interfaces of water and mineral oil are formed in the central chamber. One of these interfaces is formed at the top of the inside central column. By raising or lowering one of the reservoirs this interface can be made to deflect into the form of a bubble. A sight glass and cross hair is provided so that a reference position of this bubble can be marked. Whenever a difference in pressure is applied across the gauge, the bubble deflects. The amount of tilting of the gauge necessary to bring the bubble back to the reference height then indicates the pressure difference applied.

The reservoirs are 2 inches in diameter and 13 inches apart. The tilting of the gauge which is a measure of the relative movement of one reservoir with respect to the other is measured by a micrometer screw fitted with a scale. With a knowledge of the distance between the reservoirs, pitch of the micrometer screw, and leverage of tilting the readings of the micrometer scale can be converted into pressure units. An advantage of this instrument is that it is an absolute standard and does not have to be calibrated against any other instrument before use. Its sensitivity is 0.00065 inches of water.

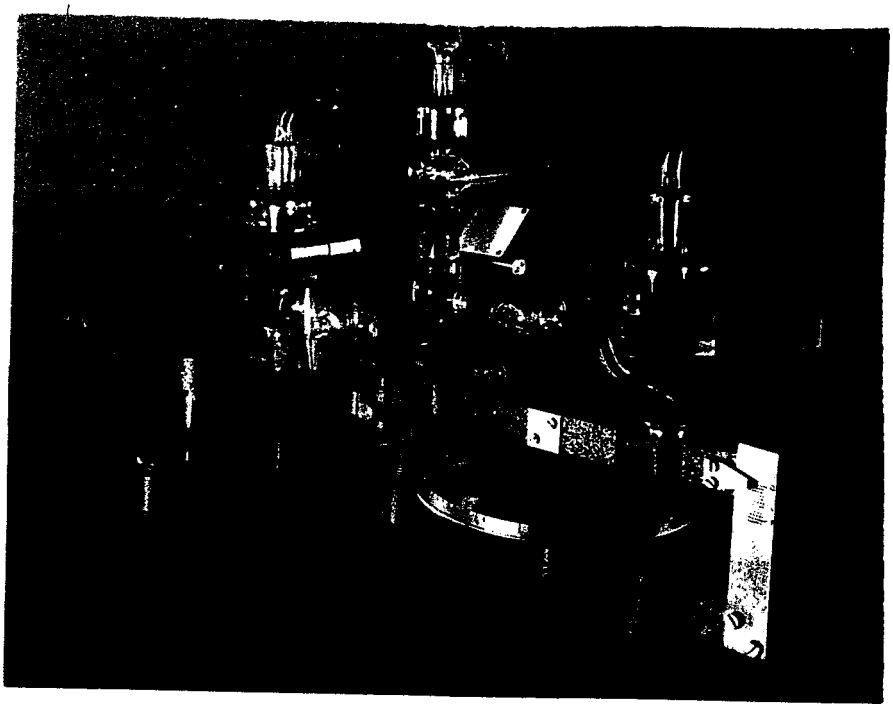

Figure 10. Chattock-Fry Tilting Manometer.

The Chattock-Fry manometer was used for all final pressure readings. Prior to this mainstream pressures were monitored by use of a micro-manometer. Mainstream total and static pressures were taken at the inlet to the test section. The total pressure was sensed by a NACA Keil-type probe. The Keil-type probe is fairly insensitive to alignment with the flow. The total pressure at the leading edge of the plate was also taken with a Keil-type probe.

5. Temperature Recording

The mainstream stagnation temperature was recorded on a Leeds-Northrup potentiometer, Model 8662, using an iron-constantan thermocouple junction with the reference junction in an ice water bath.

D. Experimental Program

As previously mentioned, the experimental program consisted of visualization techniques and static pressure measurements. The procedure used in each technique and the results obtained for that technique are reported under each subheading.

1. China Clay Technique

The technique which is commonly referred to as china clay is to immerse kaolin powder in methyl salicylate. The immersion is then applied to the airflow surface. When air flows over the surface the methyl salicylate moves across the surface and carries with it the kaolin powder. Supposedly, as in this case, the methyl salicylate would move back until separation is reached. The methyl salicylate then evaporates and leaves deposits of kaolin powder. The separation line can then be determined by studying the deposits of kaolin powder.

The results of this technique in indicating the separation point were not successful, due primarily to the application. However, some knowledge was obtained about the flow behavior in the separated region.

In indicating the separation point the methyl salicylate did not appear to move back far enough along the plate. Free stream air velocities of about 40 ft. per second were used. It was necessary to wet the surface of the plate very well with the solution in order to get the solution to flow. However, as is peculiar to this configuration, the vortex in the corner also moved the solution out from the corner forward toward the separation point. The result was that the solution from the front part of the plate met the solution from the corner part of the plate to form an area of heavier solution. Now the surface tension which resulted from this build up of solution appears to have destroyed the sensitivity of the technique at the separation point. Configurations number 1 and number 2 were used in this technique and some of the results are shown in Figure 11.

However, two things appear from this set of experiments. The first is that the flow over the surface of the plate seems to be two-dimensional. This is indicated by the heavy deposit of kaolin powder which forms in approximately a straight line across the plate. The second is the length of time necessary to dry the solution in the center of the plate. Even when the plate was lightly wetted the center area of the plate (the area near and just behind the separation line) required five times as long to dry as the areas in front of separation

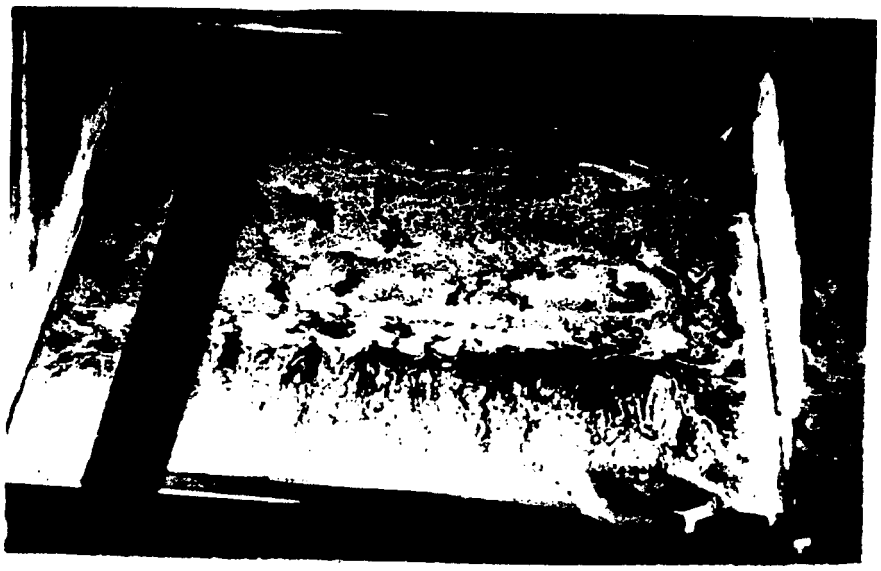

Figure 11a. China Clay Pattern With Configuration Number 1.



Figure 11b. China Clay Pattern With Configuration Number 2.

and in the corner. One explanation of this could be that in this area of the plate the flow is fairly stagnant. This sequence of drying is shown in Figure 12.

2. Smoke Traces

In an effort to get an idea of the flow behavior in the corner region pictures were taken of smoke traces. The pictures were taken with a Crown graphic camera. Configuration number 1 was used for this study. The plate surface was blackened and extraneous light was blocked out by the use of cardboard flaps. The smoke was highlighted from above by means of a spot light. The smoke was introduced into the airstream at about 2-1/2 inches ahead of the leading edge of the horizontal plate. The pictures in Figure 13 were taken at a free air stream velocity of about 4 ft. per second and configuration number 1 was used. These pictures show very clearly the vortex which exits in the corner region.

It is important to note that there appears to be a thin area of little activity between the front of the vortex and what would appear to be the separation line. It is also possible to pick out a separating streamline along this region which flows up over the vortex and seems to attach itself to the obstacle about three quarters of the way up the obstacle.

The vortex is moving in a clockwise rotation, and although it is difficult to discern it from the photographs, the smoke can fill out the vortex nearly all across the corner. In some cases where an ample supply of thick white smoke was being generated it was possible to see a tight spiral which ran from the center of the plate where the smoke



Figure 12a. Drying Pattern of China Clay After Five Minutes of Elapsed Drying Time.



Figure 12b. Drying Pattern of China Clay After Ten Minutes of Elapsed Drying Time.



Figure 12c. Drying Pattern of China Clay After Twenty Minutes of Elapsed Drying Time.



Figure 12d. Drying Pattern of China Clay After Thirty-Five Minutes of Elapsed Drying Time.



(a)



(b)

Figure 1[illegible]. Photographs of Smoke Traces Highlighting the Vortex Region.



(c)



(d)

Figure 2 (Cont'd). Photographs of Smoke Traces Highlighting the Vortex Region.



(e)



(f)

Figure 13 (Cont'd). Photographs of Smoke Traces Highlighting the Vortex Region.

was being trained, out along the corner and then up and over the obstacle along the channel sidewalls. The vortex appears to be fed from the top near the obstacle.

As the velocity of the mainflow was increased, the flow in the corner region appeared to consist of more than one vortex. The author was unable to obtain smooth streamlines in the separated region at velocities much higher than 4 ft. per second. At a higher velocity two vorticies appeared, the large one in the corner and a much smaller one in front of it. At even higher velocities the separated region appeared to become turbulent because the smoke diffused very rapidly and no vortex pattern emerged, although the general shape and size of the separated region remained the same.

3. Talcum Powder and Oil Technique

All three configurations were used for this study. The iron pipe container was filled about 3/4 full of talcum powder. The air was supplied from a shop air line. The results are shown in Figures 14a-c and listed below. The mainstream air velocity was about 20 ft. per second.

Configuration	b/h	Mainstream Velocity
1	2.42	20.3 ft/sec.
2	2.91	20.4 ft/sec.
3	1.47	20.9 ft/sec.

The procedure was to wet the surface of the horizontal plate very slightly with a light machine oil. Then the mainstream airflow was adjusted to the desired velocity. Next the talcum powder spray tube was



Figure 14a. Talcum Powder and Oil Technique for Configuration Number 1.

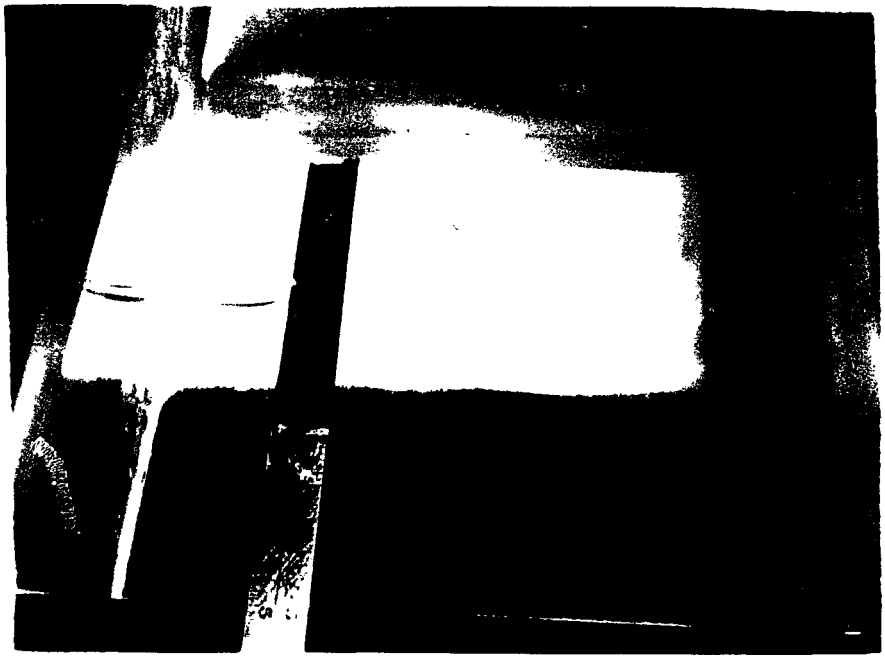

Figure 14b. Talcum Powder and Oil Technique for Configuration Number 2.

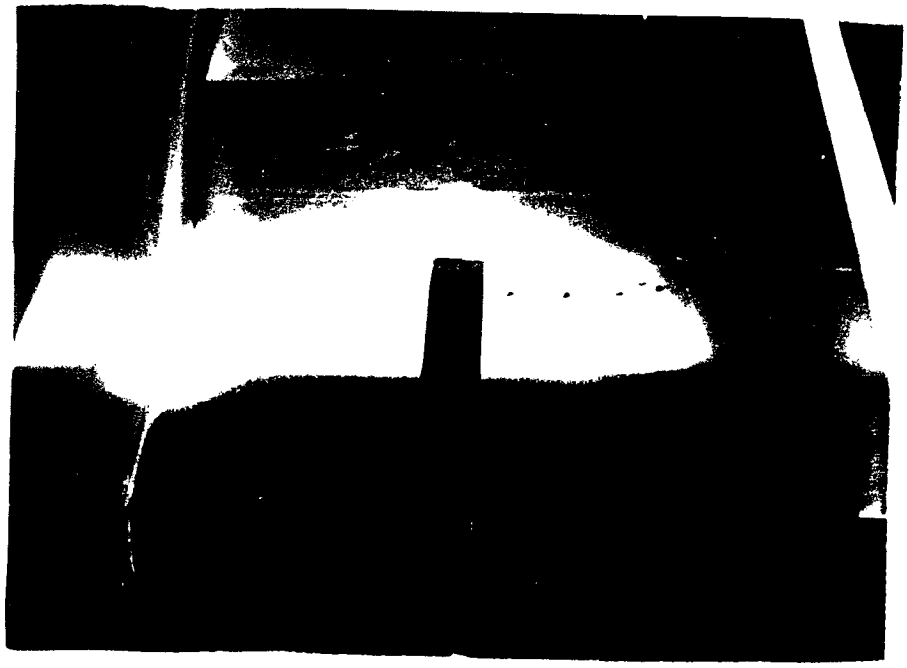

Figure 14c. Talcum Powder and Oil Technique for Configuration Number 4.

inserted through the side wall in the vicinity of the corner, (see Figure 14). The shop air supply was turned on and the iron pipe which contained the talcum powder was shaken gently to help entrain the powder in the air. The spray tube, which is bent at the end, was pointed forward a little and down toward the plate's surface. This allowed the talcum powder to spread out over the surface of the plate in the separated region. The strength of the vortex and the velocity of flow in the separated region can be appreciated by this technique. The talcum powder which did not adhere to the plate was immediately swept from the separated region up over the obstacle and downstream. The spray tube was moved across the corner region so that the talcum powder covered as much of the plate span as possible. Then the tube was removed and inserted in a corresponding hole in the opposite side wall. The operation of spraying powder was repeated from this side and areas of the plate that were not covered previously were hit.

Care had to be used with this technique and the operation repeated many times to get the proper adjustment of shop air pressure. The shop air pressure controlled the velocity of flow from the tube discharge. If the velocity of flow was too high and shaking of the talcum powder container too vigorous then a slug of powder would come out. This would carry across the plate's surface and forward ahead of separation. If the velocity was too low then the powder would be swept from the vortex before it could be deposited on the plate's surface.

Many attempts were made with the same configuration. After it was felt that the operation was successful, the results were repeated. In a successful run the talcum powder would issue from the tube discharge

and flash out through the vortex. Some of the talcum powder would become entrained in the vortex region behind the tube discharge. By looking down on the surface of the horizontal plate the vortex region all across the plate was momentarily visible. It appeared to be of about the same size as that for the smoke studies.

4. Static Pressure Measurements

All three configurations were evaluated with this technique. As previously explained great care was taken to remove any burrs or surface effects from around each hole. The pressure of the hole closest to the leading edge was used as a reference against which all other static pressures along the plate surface were measured. Therefore, the pressure from the number one static pressure hole was led to one side of the Chattock-Fry manometer and all of the other static pressures were led in turn to the other side of the manometer. The air velocity in the mainstream just beyond the discharge of the contraction section was measured with a Keil-type probe for total pressure and a static pressure tap located about 1-1/2 inches from the probe. Both were mounted in the top of the test channel. The Keil probe was also used to measure the total pressure at the leading edge of the horizontal plate. The probe was mounted from the bottom of the channel and to one side of the static pressure holes so that it would introduce no interference. Also the gauge pressure of the number one static pressure hole was taken. This enabled the calculation of gauge static pressures all along the plate.

The mainstream velocity was about 20 ft/sec. At lower velocities it was difficult to obtain accuracy of measurement because of the

smaller pressure rise. This is especially true near the leading edge with configurations number 2 and 3.

It was realized that a static pressure reading with zero error could not be obtained directly (Reference 30). Contributing factors are the finite size of the hole, the sharpness of the corner of the hole, any surface effects such as burrs, and interference upon a hole due to the disturbance of an adjacent hole. In order to find a correction for these effects, it was decided to run air over the test surface when no obstacle was present at corresponding velocities. The static pressure taps were located over a 3.0 inch span in the direction of flow. With a mainstream velocity of 20 ft/sec. and laminar flow it was felt that the pressure drop along the plate would be incidental to other effects present. Another difficulty was in obtaining a true static pressure anywhere, against which the other static pressures could be measured. As will be shown later the ratio of the difference between total and static pressures was the ultimate goal. By assuming these pressures to be corrections from atmospheric pressure, the small error introduced would eventually be minimized. The pressure corrections of Figure 15 are, therefore, the difference between the measured pressure and atmospheric pressure.

The corrections were applied as indicated. Then a corrected static pressure variation along the horizontal plate for configurations 1, 2, and 3 was plotted versus position along the plate from the leading edge. (See Figures 16, 17, and 18.) Since the theoretical results were set up in terms of the leading edge velocity, it was desirable to obtain the leading edge static pressure. When this was combined with the total

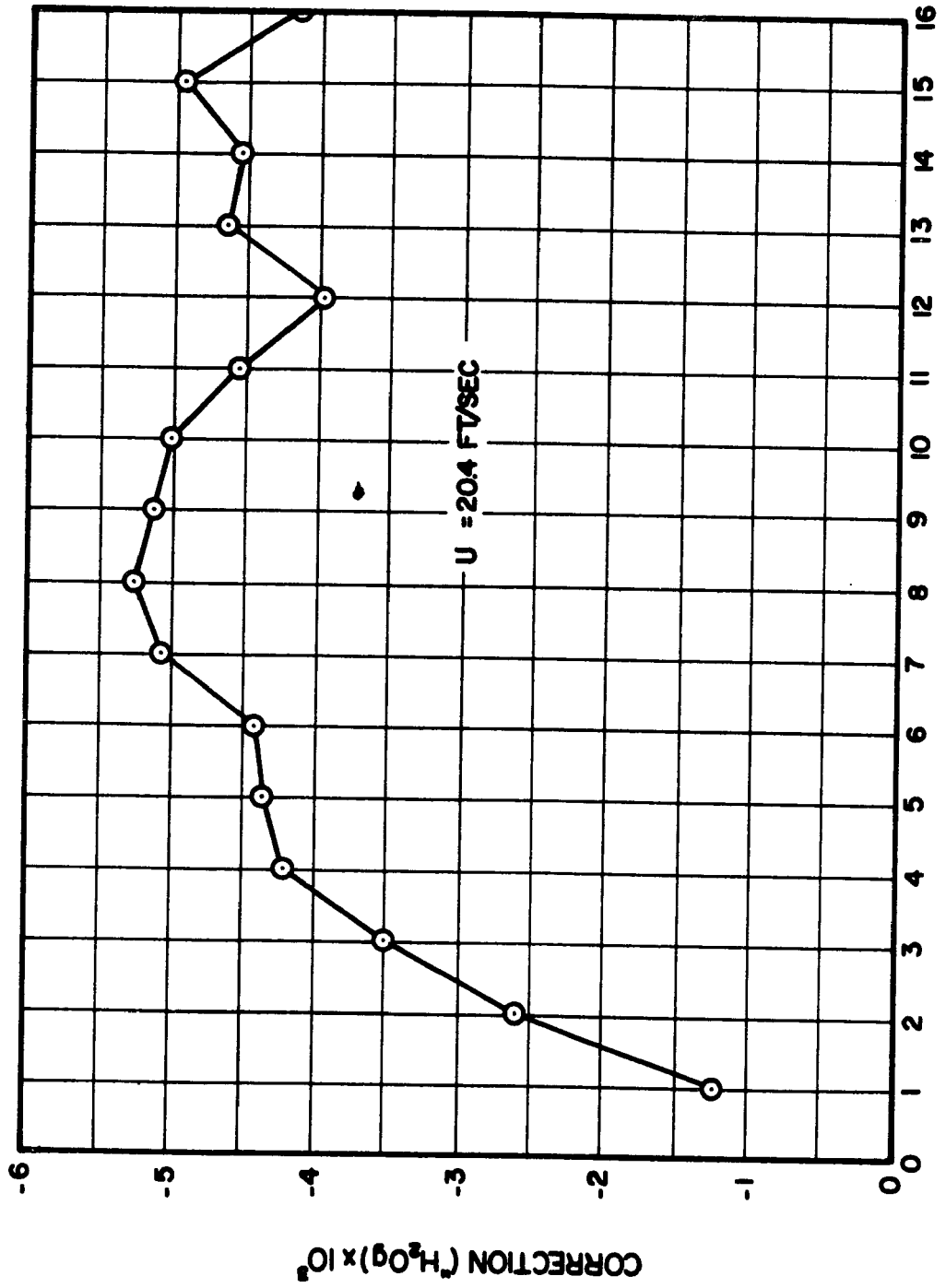

Figure 15. Static Pressure Correction vs. Hole Number.

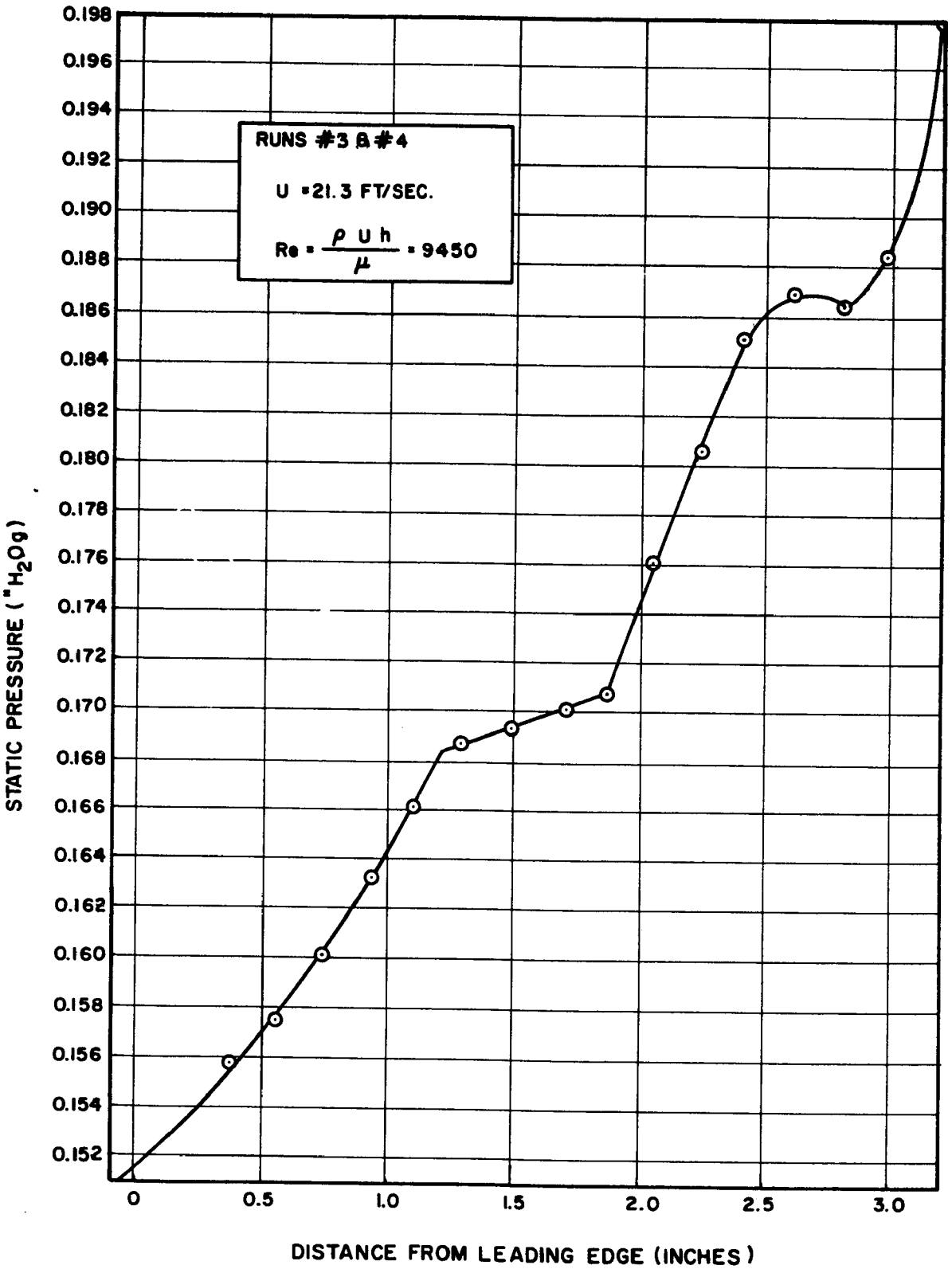

Figure 16. Static Pressure Variation Along Horizontal Plate of Configuration Number 1.

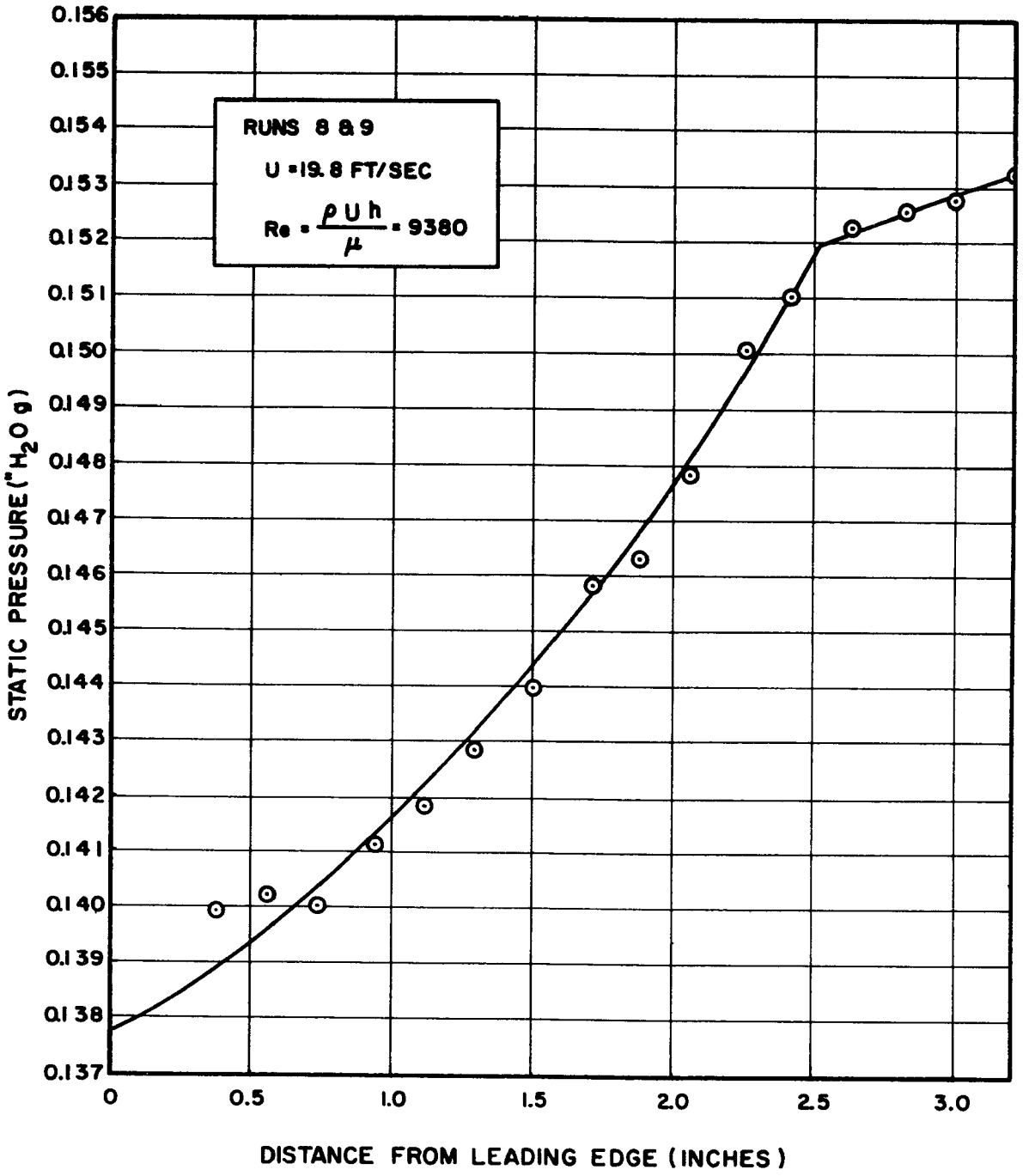

Figure 17. Static Pressure Variation Along Horizontal Plate of Configuration Number 2.

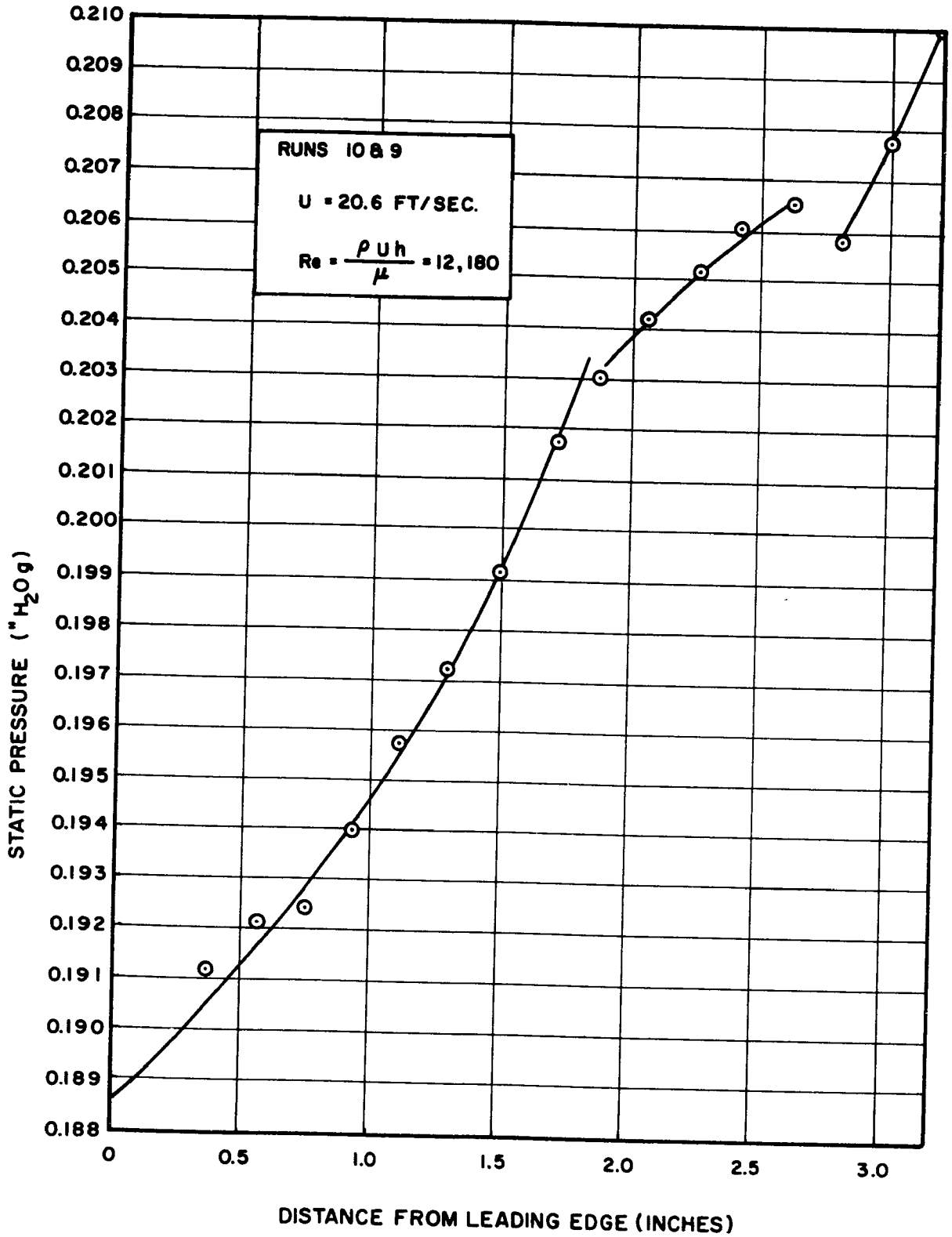

Figure 18. Static Pressure Variation Along Horizontal Plate of Configuration Number 3.

pressure at the leading edge it gave the leading edge velocity. Therefore, the curve of static pressure variation was extrapolated to the leading edge. Assuming that the mainstream total pressure did not vary ahead of separation, then Bernoulli's equation gives

$$P_T - P = \frac{\rho}{2} U^2$$

If $P_T - P_o$ represents the difference between the total and static pressures at the leading edge, then a dimensionless free stream velocity variation along the plate can be determined from

$$\bar{U} = \sqrt{\frac{P_T - P_n}{P_T - P_o}} \qquad (101)$$

where P_n represents the corrected static pressure at the n-th static pressure hole. In this way the free stream velocity variation along the horizontal plate was obtained for the three configurations. The results are shown in Figures 19, 20, and 21.

Referring to Figures 16, 17, and 18 it is seen that in each case a sharp change of slope of the static pressure variation occurs. This change occurs at different places for all three configurations. For configurations number 1 and 3 where the static pressure holes extended the full length of the horizontal plate two sharp changes appear. The erratic behavior in the very corner is probably due to picking up part of the dynamic head as the vortex sweeps down the obstacle and along the plate. The explanation for the sharp breaks is that the first break indicates separation. The flat portion of the curve which indicates a small pressure rise could be due to a region of fairly stagnant flow.

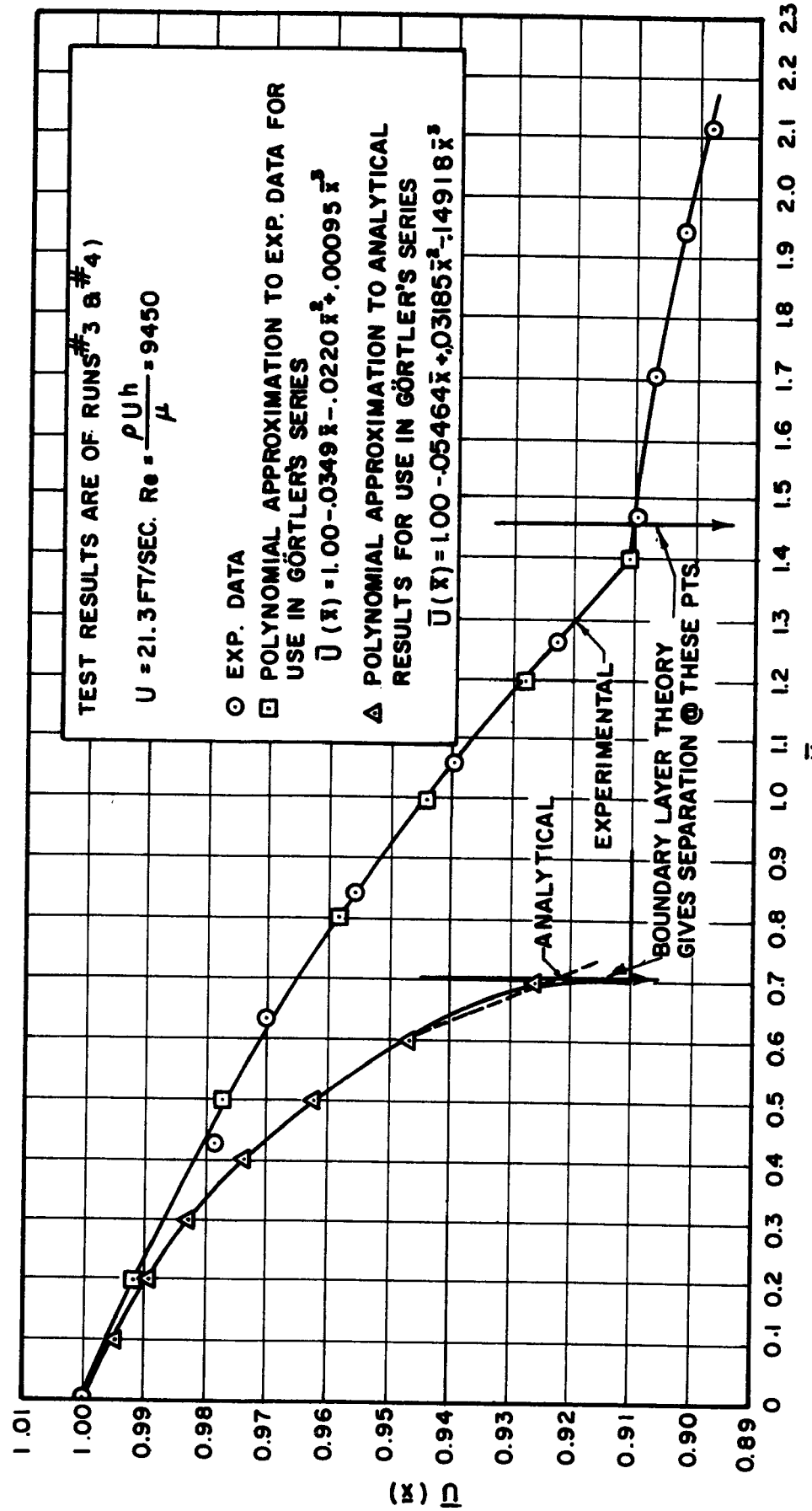

Figure 19. Plot of Dimensionless Velocity vs. Dimensionless Distance for Analytical and Experimental Results of Configuration Number 1.

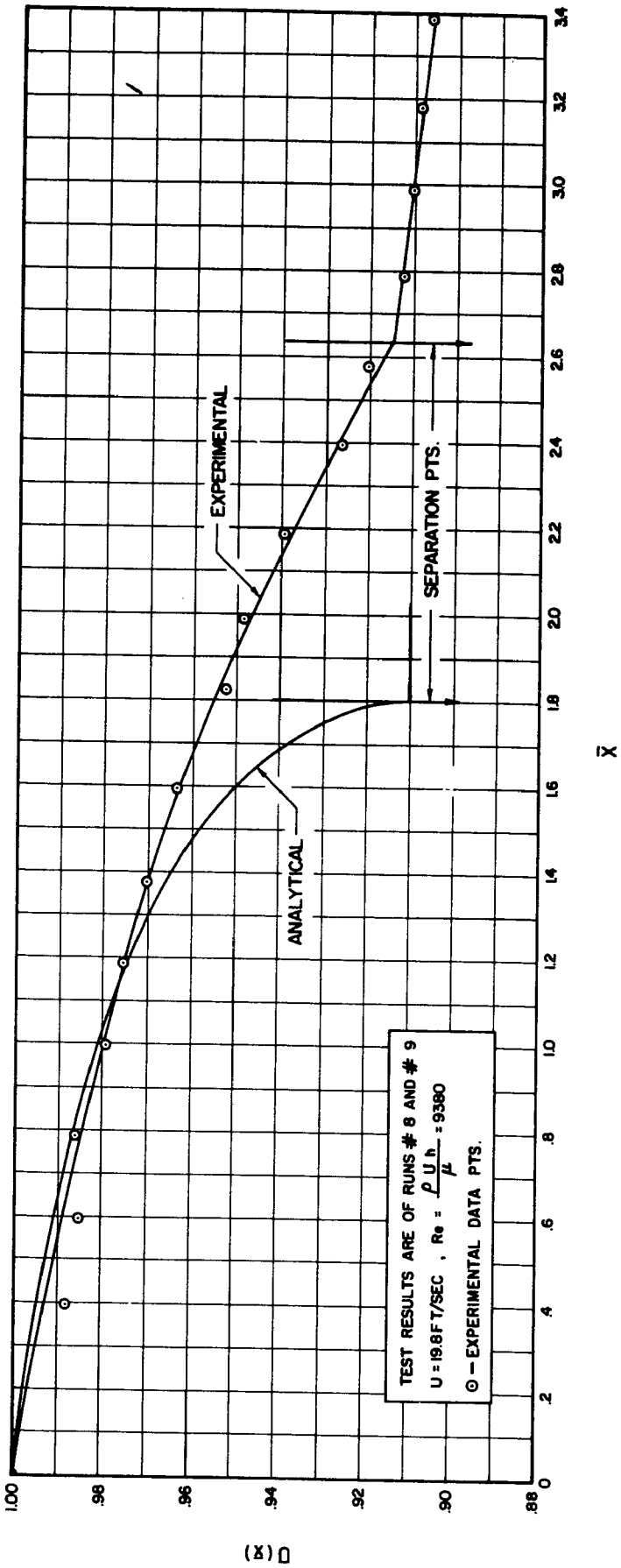

Figure 20. Plot of Dimensionless Velocity vs. Dimensionless Distance for Analytical and Experimental Results of Configuration Number 2.

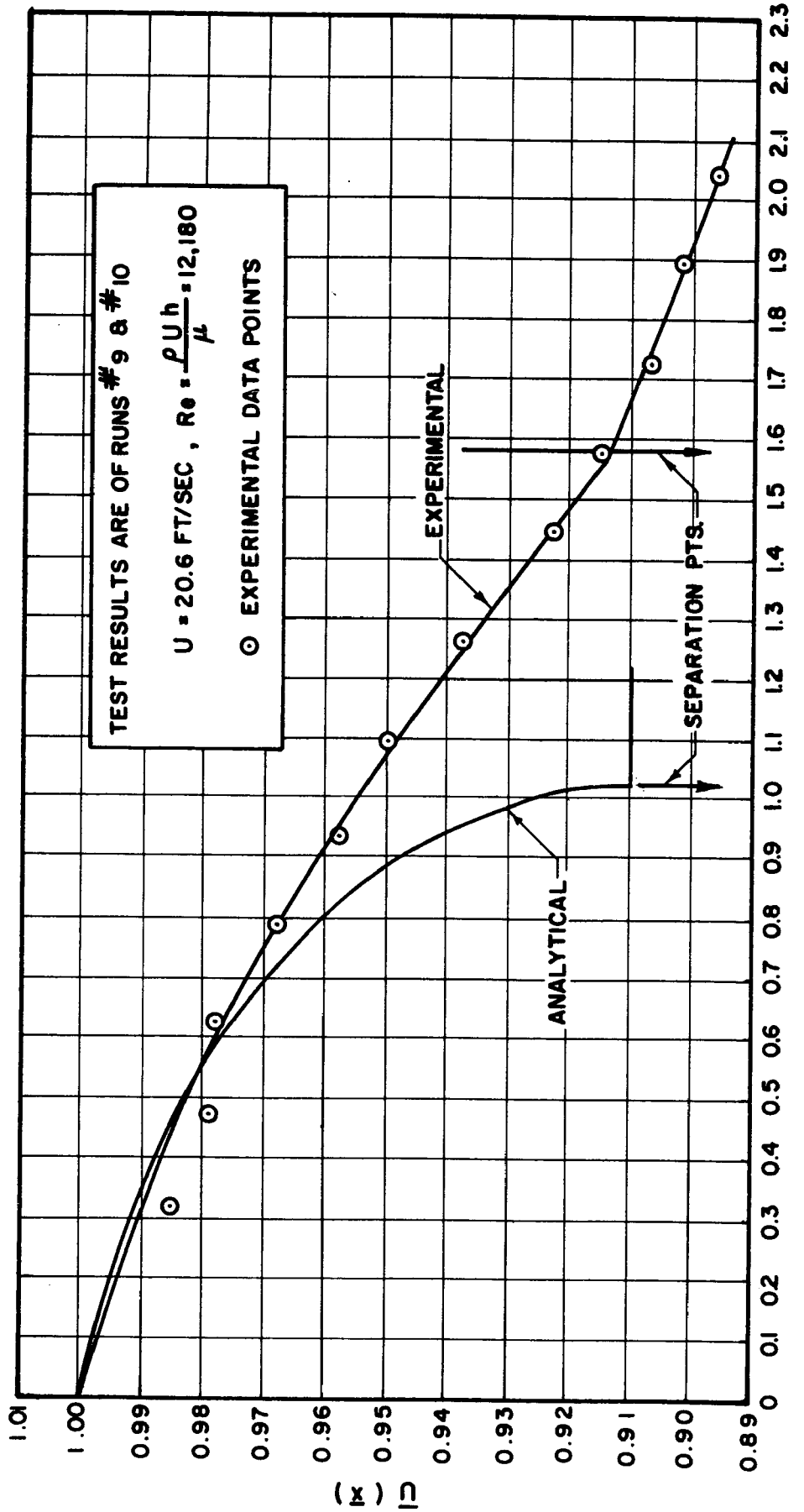

Figure 21. Plot of Dimensionless Velocity vs. Dimensionless Distance for Analytical and Experimental Results of Configuration Number 3.

This has been indicated before during the china clay and smoke studies. The last break and subsequent steep pressure rise is due to the vortex which exists in the corner region. Its flow as previously mentioned is forward along the plate surface.

The Figures 19, 20, and 21 also include a plot of the theoretical free stream velocity variation from the leading edge back to the theoretical separation point. This was done so that a direct comparison of the results, theoretical versus experimental, could be obtained.

Also in connection with configuration number 1 it was felt that the experimental free stream velocity variation should be used in Gortler's series and Witting's finite difference process in order to verify the existence of separation at the first break. Therefore, the experimental free stream velocity variation of configuration number 1 was approximated by the third degree polynomial

$$\bar{U}(\bar{x}) = 1.000 - .0349\bar{x} - .0220\bar{x}^2 + .00095\bar{x}^3 \qquad (102)$$

This plot is shown in Figure 19 by means of the small squares.

Using Gortler's series

$$\begin{aligned} \bar{u}_0 &= 1.000 \\ \bar{u}_1 &= -.0349 \\ \bar{u}_2 &= -.0220 \\ \bar{u}_3 &= +.00095 \end{aligned} \qquad (103)$$

Then

$$\begin{aligned} \bar{\beta}_0 &= 0 \\ \bar{\beta}_1 &= -.06980 \\ \bar{\beta}_2 &= -.09288 \\ \bar{\beta}_3 &= -.00539 \\ \bar{\beta}_4 &= -.00487 \\ \bar{\beta}_5 &= -.00040 \end{aligned} \qquad (104)$$

These values will then give:

$$\begin{aligned}
\bar{F}_0''(0) &= 0.469600 \\
\bar{F}_1''(0) &= -.072059 \\
\bar{F}_2''(0) &= -.087828 \\
\bar{F}_3''(0) &= -.012571 \\
\bar{F}_4''(0) &= -.009833 \\
\bar{F}_5''(0) &= -.002805
\end{aligned} \tag{105}$$

The partial sums of $(\partial\bar{u}/\partial\bar{y})|_{\bar{y}=0}$ are shown in Figure 22. It was felt that if Witting's finite difference process was employed after $\bar{x} = 1.00$, Gortler's series would still give sufficient accuracy for the calculation of velocity profiles at $\bar{x} = 1.00$ and $\bar{x} = .96$. Therefore, Witting's finite difference process was continued on from this point. ℓ was picked equal to .5915 and 18 points in the $\bar{y}$ direction were picked. The finite difference process used 7 steps in the $\bar{x}$ direction of length .04 and 8 steps of length .02. The final plot of $(\partial\bar{u}/\partial\bar{y})|_{\bar{y}=0}$ is shown in Figure 23. It indicates that separation should occur at $\bar{x} = 1.46$. This is very close to the first break as can be noted on Figure 19. This tends to verify the assumption that the break indicates the separation point.

As a result the static pressure measurements indicate the following:

Configuration	b/h	Mainstream Velocity
1	2.30	21.3 l/sec
2	2.50	19.8 l/sec
3	1.26	20.6 l/sec

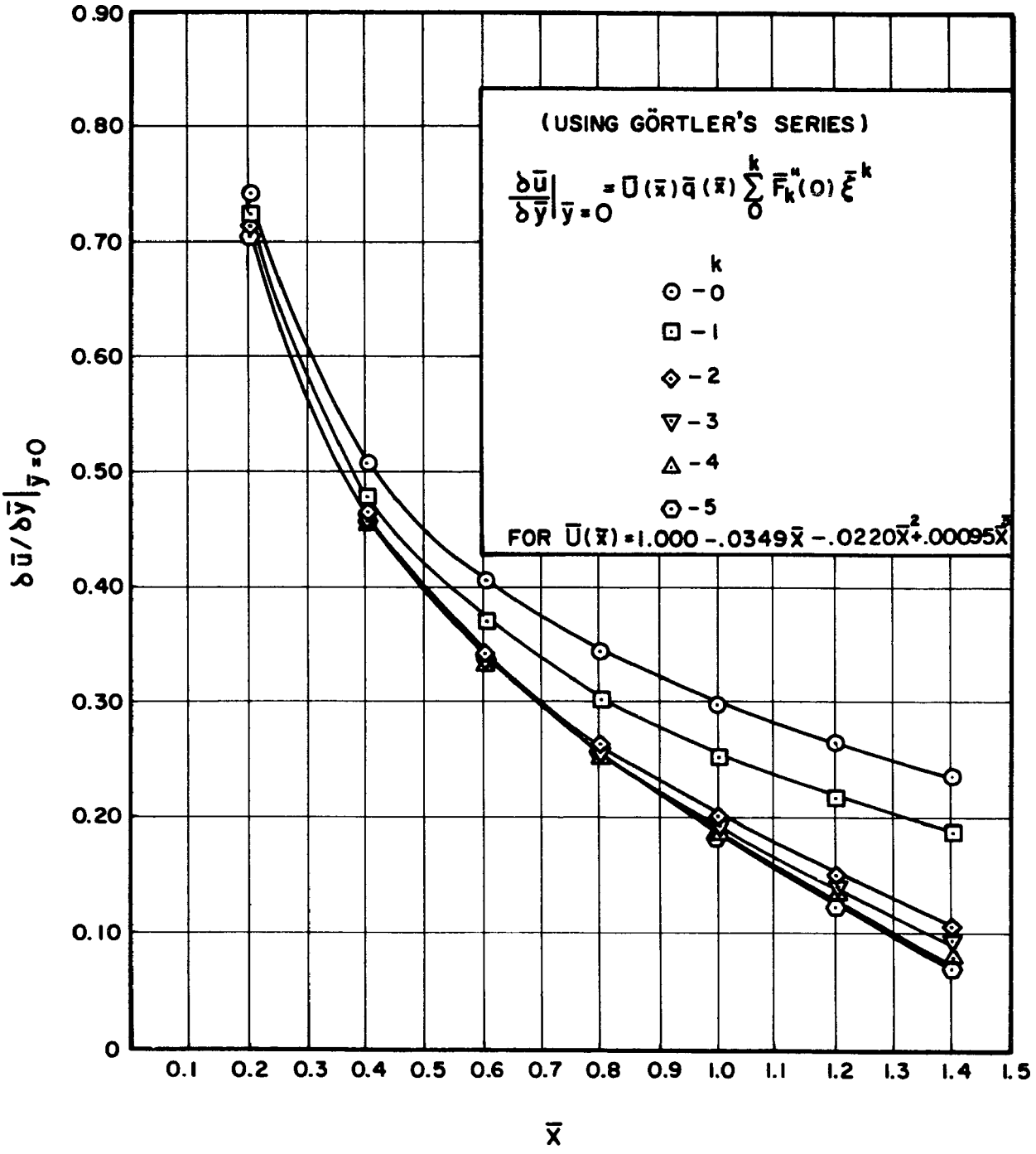

Figure 22. $\frac{\partial \bar{u}}{\partial \bar{y}}\Big|_{\bar{y}=0}$ vs. $\bar{x}$ for Configuration Number 1.

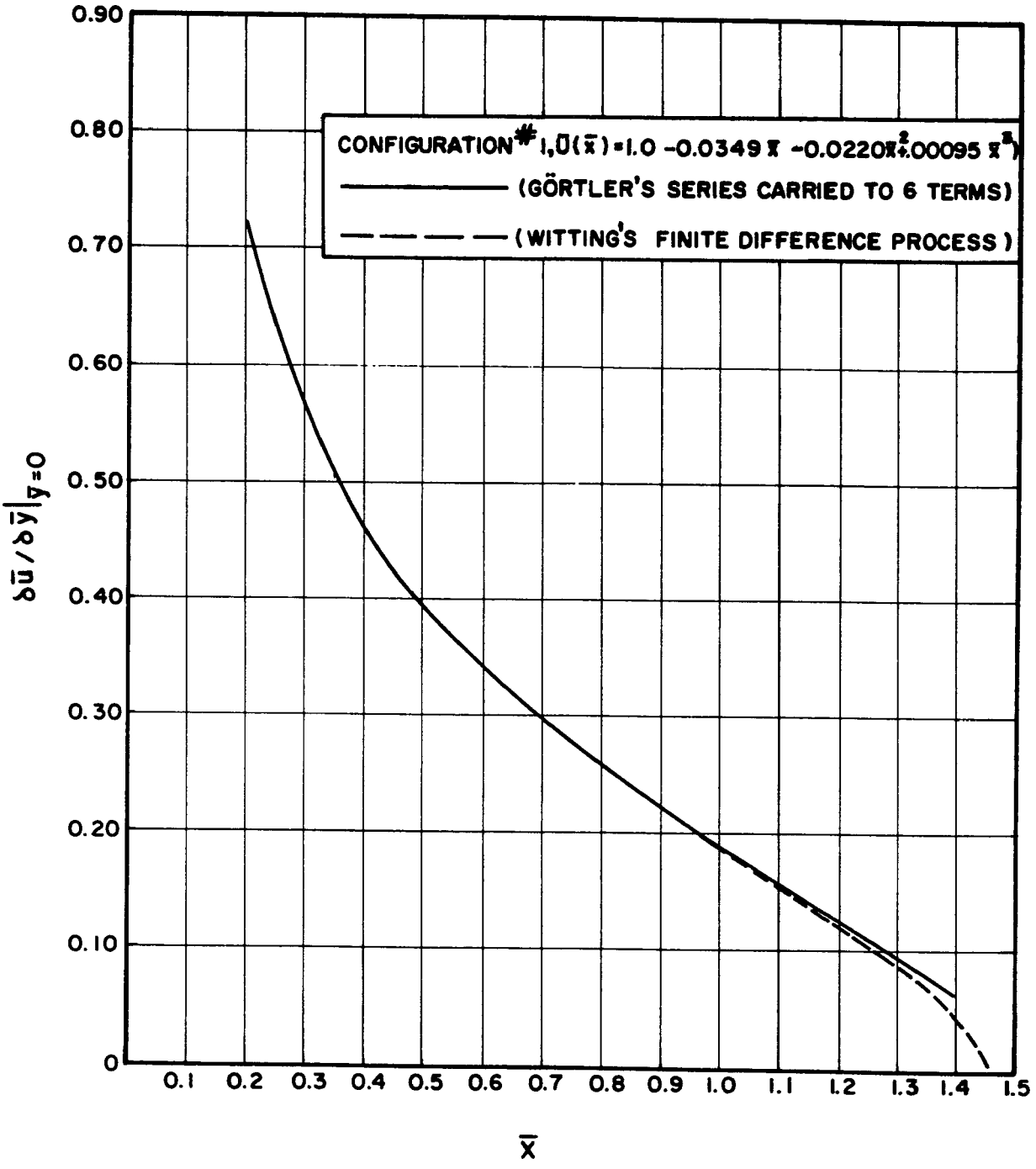

Figure 23. Plot of $\frac{\partial \bar{u}}{\partial \bar{y}}\Big|_{\bar{y}=0}$ vs. $\bar{x}$ for Experimental Velocity $\bar{U}(\bar{x})$ for Configuration Number 1.

E. Comparison of Experimental Results

The purpose of the different techniques was to produce checks upon one another. The results of the static pressure measurements and talcum powder technique are compared below:

Configuration	Static Pressure (b/h)	Talcum Powder (b/h)
1	2.30	2.42
2	2.50	2.91
3	1.26	1.47

The talcum powder indicated a separation point which was ahead of the separation point for the static pressure measurement. Of the two techniques the static pressure measurement seems more accurate. Because of the method for introducing the talcum powder into the separated region it is possible that some powder was deposited ahead of separation. This would be especially true since the velocity of flow in the boundary layer is reduced ahead of separation. Its momentum might not be sufficient to overcome any excess momentum of the talcum powder which was the result of propelling the talcum powder forward. Also, it is extremely difficult to estimate the effect upon the size of the separated region due to the cross flow component of the talcum powder. This could have a large effect and produce an enlarged region.

Using the results of the static pressure measurements the distance from the corner to the separation point appears to check very closely with the indicated separation point for the smoke studies. The separation point for the smoke studies was assumed to be where the smoke

first appeared to leave the surface of the plate, not the apparent front edge of the corner vortex. Between these two studies there appears to be good correlation. The smoke also indicates an area in which there appears to be little activity, as was indicated with the static pressures. This area of low activity was also apparent from the drying patterns during the china clay runs.

There seems to be a plausible explanation for the area of low activity. The flow which is adjacent to the surface of the plate before separation leaves the surface at separation. Considering the dynamics for a plane steady two dimensional flow, the acceleration component normal to the path of a fluid particle equals the velocity of the particle squared, divided by the radius of curvature of the path. This means that the flow must leave along a path which is tangent to the surface at separation. To do otherwise would require an infinite force normal to the path. Even a fairly steep path leaving the plate would seem unreasonable for the geometry of the flow. Now the same is true for the flow in the vortex. In order that the flow in the front edge of the vortex meet the separation point it must in either case be subjected to an infinite force. Since the mainstream flow leaves along a tangent line it is impossible for the vortex to reach all the way forward to separation. This leaves an area which is relatively stagnant between the separation point and the vortex.

Another aspect of the comparison between the smoke studies and the static pressure measurements is that the separation point seems insensitive to mainstream velocity changes as long as the flow remains laminar up to the separation point. The smoke studies which indicate laminar flow even in the vortex were made at mainstream velocities of

4 ft/sec. The static pressure measurements were taken at 20 ft/sec. and the laminar boundary layer equations were used to verify the separation point. By comparing the photographs of Figures 13a-f with the results of Figure 19, it is evident that separation appears at very nearly the same location.

CHAPTER V

RESULTS AND CONCLUSIONS

A. Results

The analysis gave the following three configurations:

Configuration	Γ	U/V	S/Y	l/h	a/h
1	90°	1.15	.97	3.70	1.00
2	90°	1.11	1.15	5.15	1.00
3	45°	1.12	1.00	2.84	.56

The results of both the analysis and the experiments for determining separation are:

Configuration	Analysis b/h	Static Pressures b/h	Talcum Powder b/h
1	3.00	2.30	2.42
2	3.33	2.50	2.91
3	1.81	1.26	1.47

Figure 24 gives a scale drawing of the configurations and shows the locations of the different separation points. The results do not indicate very good agreement between experiment and theory. The experimental results based on the static pressure measurements indicate an error of about 25%. The experimental results based on the talcum powder technique are about 16% from theoretical.

The reason for the discrepancy obviously lies in the method of analysis. In the analysis it was assumed that the fluid in the separated

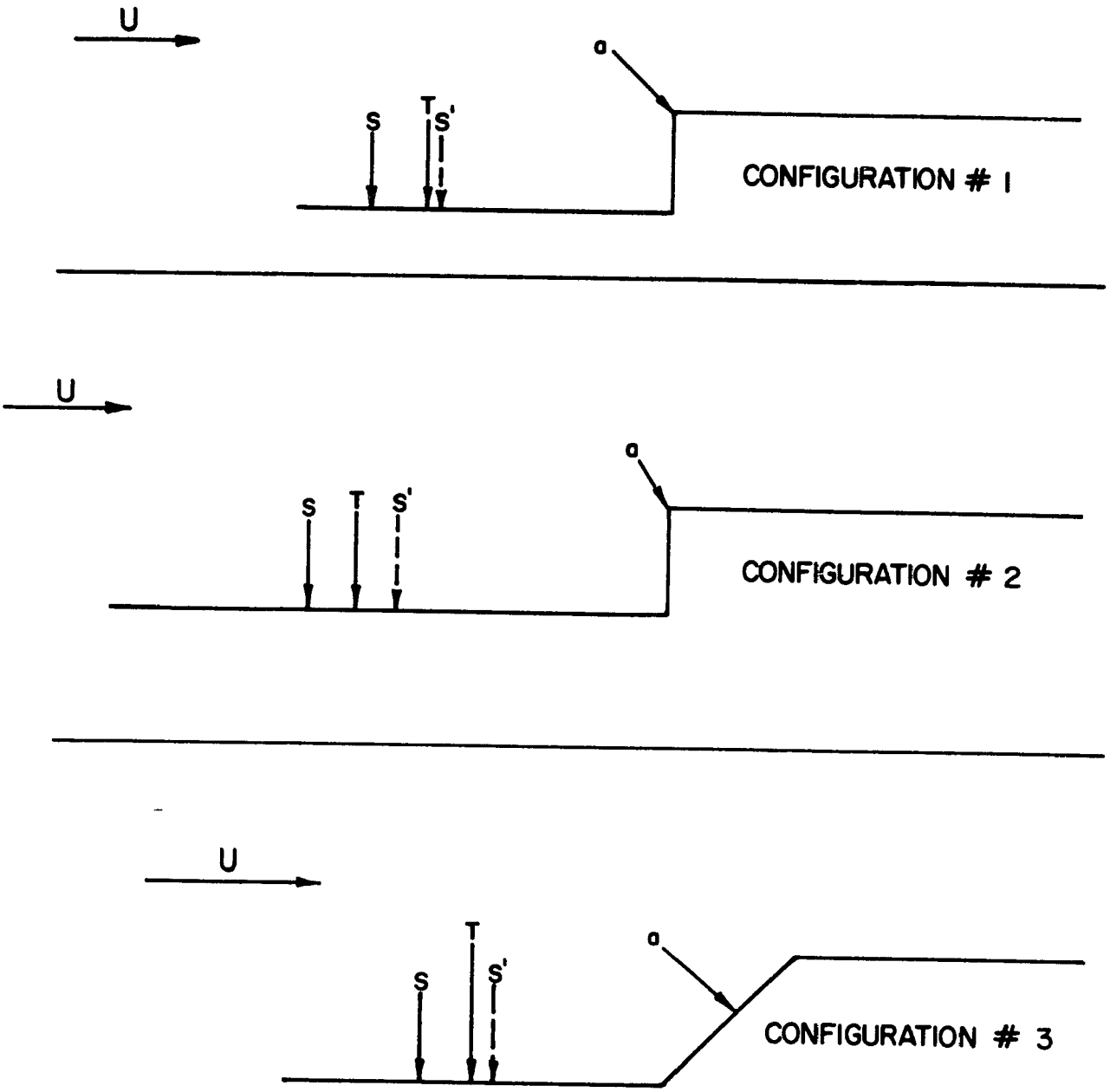

S — SEPARATION PT. - THEORETICAL
a — ATTACHMENT PT. - THEORETICAL
S' — SEPARATION PT. - STATIC PRESSURES
T — SEPARATION PT. - TALCUM POWDER AND OIL

Figure 24. Scale Drawing of the Channel Configurations, Showing Analytical and Two Experimental Separation Points.

region was stagnant or at a very low velocity compared with the outer flow. It has been shown experimentally that the region of stagnant flow lies just behind separation and extends over a very small area of the separated region. The remaining part of this region is moving in a strong vortex. It is interesting to note that Figures 19, 20, and 21 indicate that the separation velocity is approximately the same as that assumed in the potential solution. The potential solution, however, dips at separation and the velocity gradient is infinite at separation.

These discrepancies do not preclude the analysis. One of the goals of this investigation was to analyze the problem with the view of determining a first order approximation which would be useful over a wide variety of configurations. The analysis is composed of two parts, the potential solution and the viscous solution. Because of the difference between the real and the assumed flow behavior, the viscous portion of the solution gives results which are erroneous. There is nothing, however, to keep the potential solution from being fitted to the experimental results. Using the results of the static pressure measurements of configuration 1, 2, and 3, the author calculated their flow geometries. In each case separation was assumed to occur at the first break in the measured outer velocity curve. The results are tabulated below:

Configuration	Measured b/h	U/V	S/Y	Γ	Separation Velocity
1	2.30	1.24	.76	90°	.832
2	2.50	1.20	.88	90°	.836
3	1.26	1.21	.74	45	.839

These results give a new value of the separation velocity which can be used to predict separation for other geometries. It is not the author's intention to try to check this new separation velocity by use of the viscous solution. As a result of the viscous solution carried out on the static pressure measurements of configuration number 1, it is obvious that the new separation velocity could not be checked in this way. The area of separation for the analytical approach can be compared with those of the smoke studies. The free streamline for configuration number 1 with separation at $b/h = 2.30$ is shown in Figure 25. Lighthill picked the value of .91 as the separation velocity as a result of a photograph in Goldstein.[17] The photograph shows a streamline which moves over an obstacle. It is very difficult to be sure whether this streamline is that streamline associated with the flow moving adjacent to separation.

There is another value in the analysis which is verified by the experiments. In all cases tested the discrepancy from the analysis is approximately the same and always in the same direction. This verifies the analysis as a first order approximation.

With the configurations analyzed and tested plus Lighthill's results for the infinite fluid case, the following qualitative statements can be analytically predicted and experimentally proven.

(1) For a given L/h and h/Y, decreasing Γ, the angle of the obstacle, will decrease the size of the separated region and move the separation point back along the horizontal plate.

(2) For a given L/h and Γ, increasing h/Y or decreasing the channel depth will decrease the size of the separated region and move the separation point back along the horizontal plate.

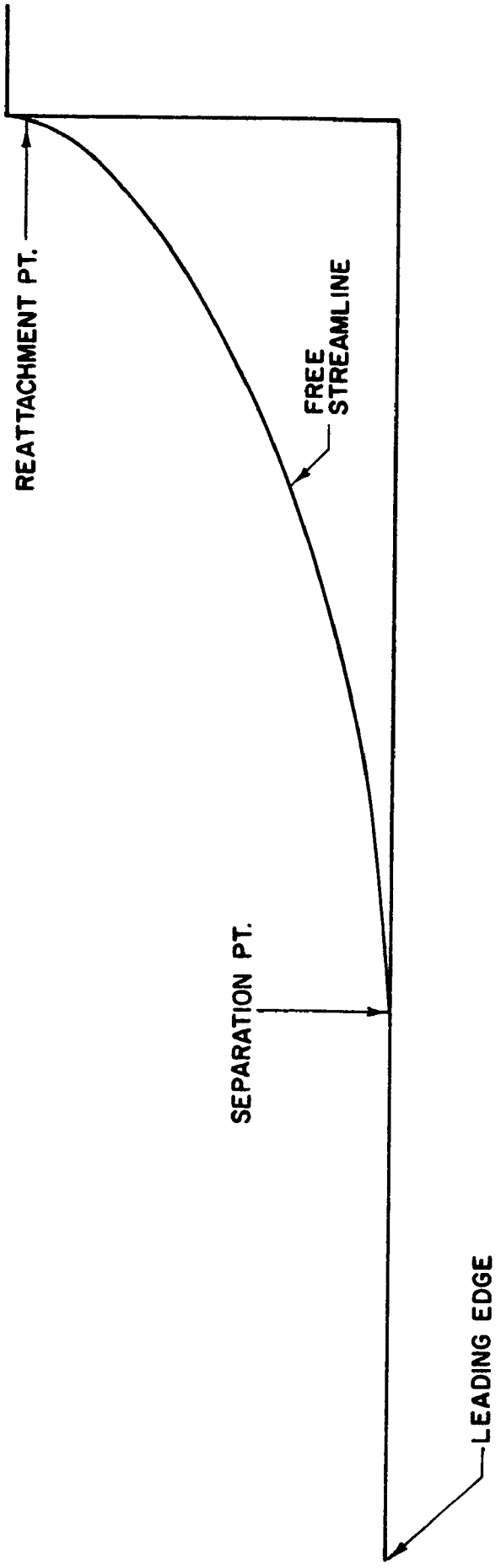

Figure 25. Plot of Free Streamline for Configuration Number 1 Using Static Pressure Test Data.

(3) For a given h/Y and Γ, increasing l/h or increasing the horizontal plate length will move the separation point forward along the horizontal plate.

B. Conclusions

1. The potential solution plus the viscous solution give results which do not agree quantitatively with the experimental results for the assumed separation velocity.

2. The potential solution can give results which agree quantitatively with the experiments if the separation velocity is assumed to be .84.

3. As a result of the configurations studied and tested plus Lighthill's infinite fluid case, the approach can be successfully applied to a wide variety of configurations involving two-dimensional flow separation.

BIBLIOGRAPHY

1. Von Kármán, Th. and Millikan, C.B., On the Theory of Laminar Boundary Layers Involving Separation, NACA Rep. No. 504, 1934.

2. Schubauer, G.B., Airflow in a Separating Laminar Boundary Layer, NACA Rep. 527, 1935.

3. Nikuradse, J., Untersuchungen ueber die Stroemungen des Wassers in Konvergenten und Diebergenten Kanalen, Forschungsarbeiten des VDI, No. 289 (1929).

4. Abramowitz, M , "On Backflow of a Viscous Fluid in a Diverging Channel". J. Math. Physics, 28, 1-21 (1949).

5. Maskell, E.C. Flow Separation in Three Dimensions, Royal Aircraft Establishment, Report No. Aero. 2565, Nov. 1955.

6. Schlichting, H., Boundary Layer Theory, Chapt. XX, Permagon Press, 1955.

7. Herzig, H.Z., Hansen, A.G., and Costell, G.R., Visualization of Secondary Flows Phenomena in Blade Rows, NACA RME52 H26, 1952.

8. Herzig, H.Z., and Hansen, A.G., "Visualization Studies of Secondary Flows with Applications to Turbomachines", Trans. of Amer. Soc. of Mech. Eng., April 1955.

9. Herzig, H.Z., and Hansen, A.G., "Experimental and Analytical Investigations of Secondary Flows in Ducts", Journal of Aero. Sci., March 1957.

10. Carrier, G.F., "The Boundary Layer in a Corner", Quart. Appl. Math., 4, 367-370 (1947).

11. Dean, W.R., and Montagnon, P.E. "On the Steady Motion of Viscous Liquid in a Corner", Proc. Cambridge Philos Soc, 45, 389-394 (1949).

12. Sowerby, L., "Flow of Fluid Along Corners and Edges" Quart.Journal of Mech. and Appl. Math., 6, 50 (1953).

13. "D-Stroemungslehre", Gamm Wissenschaftliche Jahrestagring, Hannover, May 19-20, 1959 ZAMM, (Sept. Nov. 1959), 428-453.

14. Oman, R., Three-Dimensional Laminar Boundary Layer Along a Corner, ScD. Thesis submitted MIT, Feb. 1959.

15. Batchelor, G.K., "On Steady Laminar Flow with Closed Streamlines at Large Reynolds Number", J. Fluid Mech., 1, 177, (1956).

16. Lighthill, M.J., "On Boundary Layers and Upstream Influence", Proc. Royal Soc. A., No. 1130, 217, 344, (May 1953).

17. Goldstein, S. ed. Modern Developments in Fluid Dynamics, Clarendon Press, 1938.

18. Thwaites, B. ed. Incompressible, Aerodynamics, Clarendon Press, 1960.

19. Villat, H. Ann. Ec. Normale, t.31, Paris 1914.

20. Thiry, R. Ann. Ec. Normale, t.38, Paris 1921.

21. Odquist, F.K.G., Arkiv for Mathematik Astronomi och Fysik, B 19, Stockholm 1927.

22. Byrd, P.F. and Friedman, M.D., Handbook of Elliptic Integrals for Engineers and Physicists, Springer-Verlag 1954.

23. Bowman, F., Introduction to Elliptic Functions with Applications, John Wiley & Sons, Inc., 1953.

24. Spenceley, G.W. and Spenceley, R.M., Smithsonian Elliptic Functions Tables, Smithsonian Inst., 1947.

25. Görtler, H., "A New Series for the Calculation of Steady Laminar Boundary Layer Flows", J. Math. Mech., 6, 1-66 (1957).

26. Görtler, H., Zahlentafeln universeller Funktionen zur neuen Reihe fuer die Berechnung laminarer Grenzschichten, Deutsche Versuchsanstalt fuer Luftfahrt E.V., Bericht Nr. 34, 1957.

27. Görtler, H., "Ein Differenzenverfahren zur Berechnung laminarer Grenzschichten". Ing.-Arch., 16. 173 (1948).

28. Witting, H., Verbesserungen des Differenzenverfahrens von H. Görtler zur Berechnung laminarer Grenzschichten". Dissertation Freiburg i.Br. (1953). ZAMP 4, 376-397 (1953).

29. Chang, P.K. and Dunham, W.H. Laminar Separation of Flow Around Symmetrical Struts at Various Angles of Attack, Hydromechanics Laboratory Research and Development Report, Dept. of the Navy David Taylor Model Basin, Jan. 1961.

30. Shaw, R., "The Measurement of Static Pressure", A.R.C., 20, 829, (March 1959).

31. Streeter, V.L., ed. Fluid Dynamics, McGraw Hill Book Co., 1948.

32. Milne-Thomson, L.M., Theoretical Hydrodynamics, Macmillan, 1955.